NAVAL POSTGRADUATE SCHOOL

MONTEREY, CALIFORNIA

THESIS

BIO-INSPIRED MEMS DIRECTION FINDING ACOUSTIC SENSOR FOR AIR AND UNDERWATER APPLICATIONS

by

William D. Swan

December 2016

Thesis Advisor: Gamani Karunasiri
Co-Advisor: Fabio Alves

THIS PAGE INTENTIONALLY LEFT BLANK

REPORT DOCUMENTATION PAGE			Form Approved OMB No. 0704-0188
Public reporting burden for this collection of information is estimated to average 1 hour per response, including the time for reviewing instruction, searching existing data sources, gathering and maintaining the data needed, and completing and reviewing the collection of information. Send comments regarding this burden estimate or any other aspect of this collection of information, including suggestions for reducing this burden, to Washington headquarters Services, Directorate for Information Operations and Reports, 1215 Jefferson Davis Highway, Suite 1204, Arlington, VA 22202-4302, and to the Office of Management and Budget, Paperwork Reduction Project (0704-0188) Washington, DC 20503.			
1. AGENCY USE ONLY *(Leave blank)*	**2. REPORT DATE** December 2016	**3. REPORT TYPE AND DATES COVERED** Master's thesis	
4. TITLE AND SUBTITLE BIO-INSPIRED MEMS DIRECTION FINDING ACOUSTIC SENSOR FOR AIR AND UNDERWATER APPLICATIONS			**5. FUNDING NUMBERS**
6. AUTHOR(S) William D. Swan			
7. PERFORMING ORGANIZATION NAME(S) AND ADDRESS(ES) Naval Postgraduate School Monterey, CA 93943-5000			**8. PERFORMING ORGANIZATION REPORT NUMBER**
9. SPONSORING /MONITORING AGENCY NAME(S) AND ADDRESS(ES) N/A			**10. SPONSORING / MONITORING AGENCY REPORT NUMBER**
11. SUPPLEMENTARY NOTES The views expressed in this thesis are those of the author and do not reflect the official policy or position of the Department of Defense or the U.S. Government. IRB number ____N/A____.			
12a. DISTRIBUTION / AVAILABILITY STATEMENT Approved for public release. Distribution is unlimited.			**12b. DISTRIBUTION CODE**

13. ABSTRACT (maximum 200 words)

A Micro Electro Mechanical System (MEMS) directional acoustic sensor has been developed based on the coupled eardrums of the *Ormia ochracea* fly. Previous versions exploited the bending resonance of the sensor and have required two sensors in an array to resolve arrival bearing ambiguity. Design changes have been implemented to exploit an additional resonant mode of the coupled oscillator, allowing for direction finding from a single sensor. Successful testing of this single-sensor direction finding method was performed in an anechoic room using a lock-in amplifier for data capture.

Additionally, a new sensor has been designed and fabricated, along with an appropriate housing, in an attempt to explore the feasibility of using this MEMS sensor in an underwater environment. The design and construction of the housing and the new sensor are also presented in this thesis, along with initial characterization testing of the sensor response in water.

14. SUBJECT TERMS MEMS, direction finding, *Ormia ochracea*, acoustic sensor, underwater			**15. NUMBER OF PAGES** 85
			16. PRICE CODE
17. SECURITY CLASSIFICATION OF REPORT Unclassified	**18. SECURITY CLASSIFICATION OF THIS PAGE** Unclassified	**19. SECURITY CLASSIFICATION OF ABSTRACT** Unclassified	**20. LIMITATION OF ABSTRACT** UU

NSN 7540-01-280-5500 Standard Form 298 (Rev. 2-89)
Prescribed by ANSI Std. 239-18

THIS PAGE INTENTIONALLY LEFT BLANK

Approved for public release. Distribution is unlimited.

BIO-INSPIRED MEMS DIRECTION FINDING ACOUSTIC SENSOR FOR AIR AND UNDERWATER APPLICATIONS

William D. Swan
Lieutenant, United States Navy
B.S., University of South Carolina, 2008

Submitted in partial fulfillment of the
requirements for the degree of

MASTER OF SCIENCE IN APPLIED PHYSICS

from the

NAVAL POSTGRADUATE SCHOOL
December 2016

Approved by: Gamani Karunasiri
Thesis Advisor

Fabio Alves
Co-Advisor

Kevin B. Smith
Chair, Department of Physics

THIS PAGE INTENTIONALLY LEFT BLANK

ABSTRACT

A Micro Electro Mechanical System (MEMS) directional acoustic sensor has been developed based on the coupled eardrums of the *Ormia ochracea* fly. Previous versions exploited the bending resonance of the sensor and have required two sensors in an array to resolve arrival bearing ambiguity. Design changes have been implemented to exploit an additional resonant mode of the coupled oscillator, allowing for direction finding from a single sensor. Successful testing of this single-sensor direction finding method was performed in an anechoic room using a lock-in amplifier for data capture.

Additionally, a new sensor has been designed and fabricated, along with an appropriate housing, in an attempt to explore the feasibility of using this MEMS sensor in an underwater environment. The design and construction of the housing and the new sensor are also presented in this thesis, along with initial characterization testing of the sensor response in water.

THIS PAGE INTENTIONALLY LEFT BLANK

TABLE OF CONTENTS

LIST OF FIGURES

THIS PAGE INTENTIONALLY LEFT BLANK

LIST OF TABLES

THIS PAGE INTENTIONALLY LEFT BLANK

LIST OF ACRONYMS AND ABBREVIATIONS

DF	Direction Finding
ILD	Inter-aural Level Difference
ITD	Inter-aural Time Difference
MEMS	Micro Electrical Mechanical Systems
PCB	Printed Circuit Board
SEM	Scanning Electron Microscope
SOIMUMPS	Silicon-on-Insulator Multi User Manufacturing Process

THIS PAGE INTENTIONALLY LEFT BLANK

ACKNOWLEDGMENTS

This thesis is merely the next step in a long-term project to create useful technology based on a fly's ear. Mike Touse, John Roth, and Dan Wilmott have all made critically important steps before me that set me up for success. Their work continues to be a valuable reference for those of us who follow in this project.

I would like to thank my advisors, Dr. Gamani Karunasiri and Dr. Fabio Alves. Dr. Karunasiri's vision and leadership have long been vital to the progress made by all of us involved in the production and testing of this family of sensors. Dr. Alves is very nearly a magician in the laboratory and brings a career of electronics experience to bear when constructing and testing equipment.

I would also like to thank Dr. Joseph Hooper, Steve Jacobs, and Jay Adeff for technical assistance and for supporting the fabrication of materials necessary for this project's success.

Finally, I am grateful to my wife, Dehlia, for supporting me in this endeavor, and to my children, Lyra, Carina, and Vela, who are my guiding stars.

THIS PAGE INTENTIONALLY LEFT BLANK

I. INTRODUCTION

A. BACKGROUND

Human hearing makes use of the inter-aural time difference (ITD), or the difference in arrival time of a sound wave from one ear to the other, in combination with the inter-aural level difference (ILD), which is the difference in the sound pressure field between the ears, in order to determine from which direction a sound originated. In general, this is a successful direction finding (DF) strategy for an animal with ear spacing comparable to the wavelength of the incident sound, at least in the horizontal plane with respect to the ears. Human hearing can identify the originating direction of an incoming sound wave to typically 1–4 degrees of bearing accuracy by this method, depending on the type and frequency of sound generated and the number of simultaneous sources [1].

1. The *Ormia Ochracea* Fly

Ormia ochracea is a parasitic fly that has evolved the ability to accurately DF a particular cricket chirp for the purpose of laying eggs in the cricket. Unlike humans, the fly has two eardrums physically connected by a cartilaginous bridge about 0.5 mm wide and a total hearing system width of around 1.5 mm [2]. The relevant cricket chirp is around 4.8 KHz, corresponding to a wavelength of approximately 7 cm, almost two orders of magnitude longer than the eardrum separation of the fly [2].

Miles [2] identified and studied the mechanically coupled resonant mode oscillations of the *Ormia* ear drums and found that they oscillate at one frequency that excites a bending mode that responds to sound pressure amplitude and at another frequency that excites a rocking mode that responds to incident direction of the sound. He modeled the fly's hearing system as a set of coupled mechanical oscillators as shown in Figure 1. The fly appears to analyze the superposition of the two resonant oscillation modes to determine the incident direction of the cricket chirp, thus allowing for accurate DF of wavelengths significantly longer than the length scale of the hearing system.

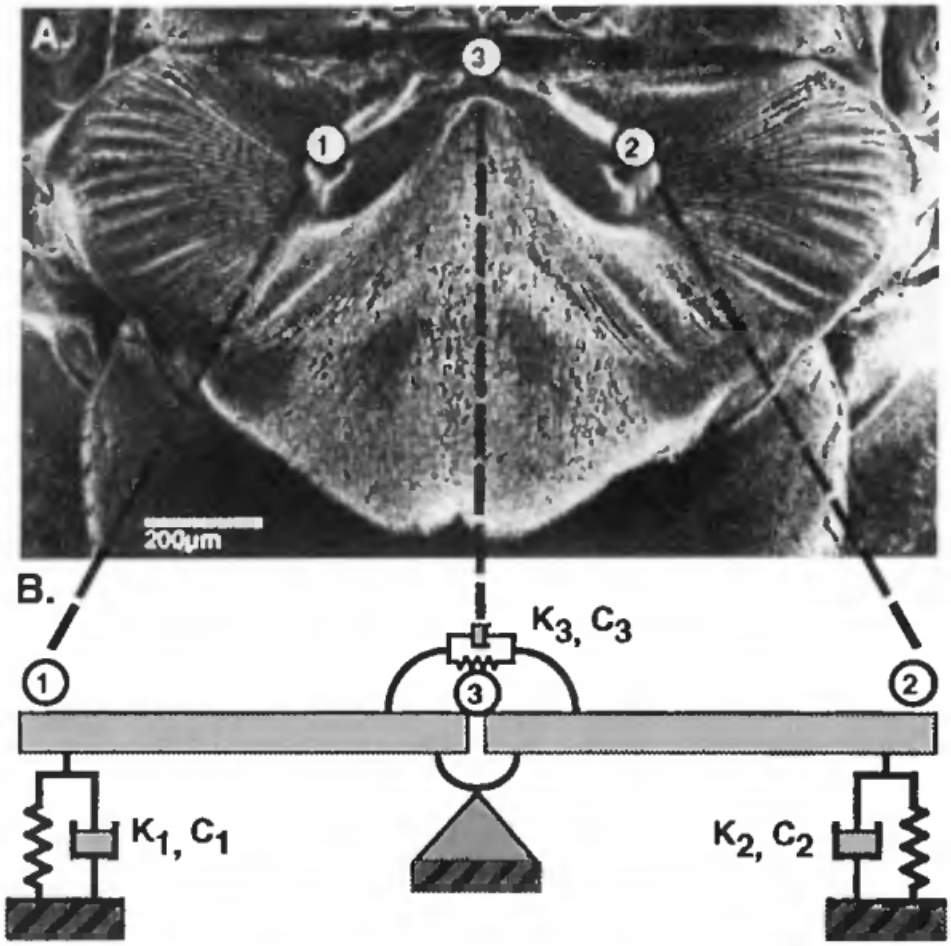

Positions 1 and 2 indicate the center of mass of the tympanal membranes. Position 3 indicates the central pivot point of the intympanal bridge. The fly's hearing system is represented as two mechanical bars connected by springs, K, and dash pots, C, modeling the dynamic properties of the actual moving components of the fly's ears.

Figure 1. *Ormia Ochracea* Hearing System and Corresponding Mechanical Model. Source: [2].

2. Development of a MEMS Sensor Based on the *Ormia* Fly

Until now, multiple researchers have contributed to the design and construction of a direction finding MEMS acoustic sensor based on the coupled oscillatory ear drums of the *Ormia ochracea* fly ear [3]–[5]. Figure 2 shows a prototypical design in which the eardrums are fashioned out of a silicon device layer with the substrate completely trenched away behind the wings, allowing free motion of the wings when subject to an acoustic pressure wave. The wings are mechanically coupled by a bridge, and they are

connected to the substrate by means of flexible torsion legs that simulate the cartilaginous connection between the eardrums in the fly.

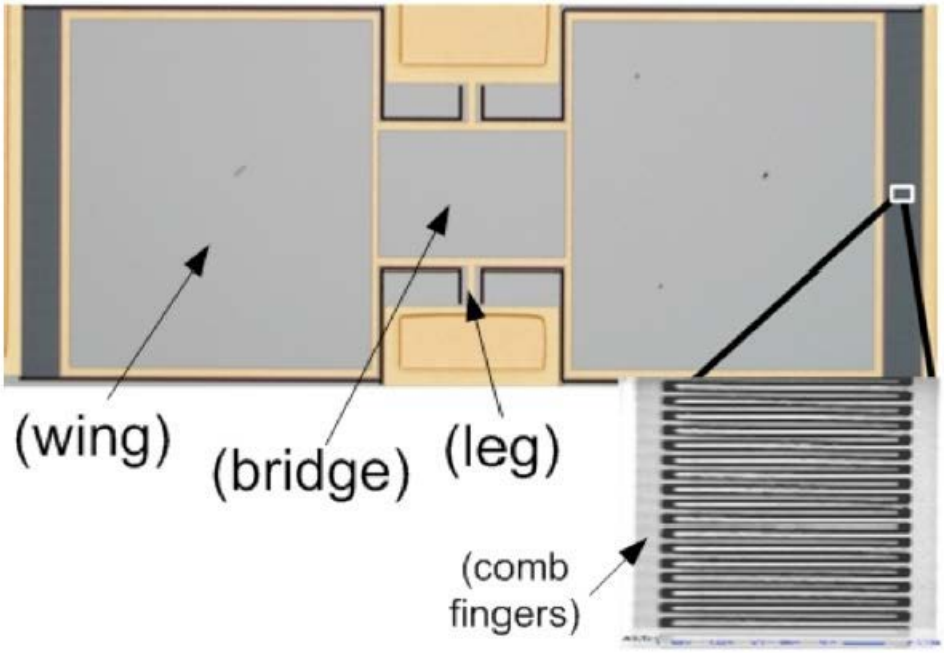

Two free-standing wings are mechanically coupled by a bridge and joined to the substrate by torsion legs. The inset zooms in on interdigitated comb finger capacitors used for sensor response readout.

Figure 2. Previous Generation MEMS Acoustic Sensor Based on the *Ormia* Fly Ear. Source: [4].

These devices have been produced by MEMSCAP using standard SOIMUMPS processing techniques [6] on a 400 micron substrate with a 25 micron device layer. Readout of the amplitude of oscillations is achieved through the use of interdigitated comb fingers around the outside edges of the wings and substrate, which form a variable capacitor. The total capacitance of the wings change as the wing oscillates with respect to the substrate [3], and this variable capacitance is compared to a reference capacitor integrated onto the MEMS device and then fed into an MS3110 Universal Capacitive Readout IC produced by Irvine Sensors [5].

The technological driver for this program has been to produce a wearable MEMS DF acoustic sensor that is accurate, fast, and light, with the goal of fielding a soldier-

mounted system to DF gunfire. A single sensor has previously been demonstrated capable of determining incident direction with a cosine dependence on arrival angle, which produces a left-right ambiguity. Most recently, Wilmott [4] constructed a two-sensor configuration able to detect incident direction of a sound wave in air over a 120-degree range with high accuracy and no arrival ambiguity in a laboratory setting.

B. OBJECTIVE AND THESIS ORGANIZATION

The objective of this thesis is twofold. First, design changes to the *Ormia* based MEMS sensor in air will be studied that allow for single sensor DF, as well as developing characterization procedures for these sensors. Second, design, construction, and testing of a novel *Ormia* based directional sensor for use underwater will be explored.

This thesis is organized in five chapters. Chapter I presents background on the *Ormia ochracea* fly hearing system and previous work done at NPS on the development of MEMS sensors based on the fly ears.

Chapter II describes the basis for design changes intended to eliminate the need for a dual sensor array and presents test results in support of those design changes. If our sensors can exploit both resonant modes similar to what the fly does, then we should, in principle, be able to DF with a single sensor. Additionally, simulations of sensor performance in this new design configuration are presented and compared to test results performed in the NPS anechoic room.

Chapter III presents the changes to the sensor required for underwater use, as well as the design and construction of an appropriate submerged housing for the sensor.

Chapter IV presents simulations of the expected performance of the new sensor design underwater and compares them with the actual results obtained in the NPS water testing facility.

Chapter V presents the assessment of the results and recommendations for further development of both sensor designs.

II. NOVEL DESIGN FOR SINGLE-SENSOR DIRECTIONALITY IN AIR

The motivation for the MEMS sensor described here derives from the study of the *Ormia ochracea* fly and its ability to DF a particular cricket chirp frequency, as first described by Miles [2]. His analysis of the resonant modes of the fly's hearing system identified two primary modes used by the fly for DF capabilities: a pure rocking mode and a pure bending mode. In all previous designs of the MEMS sensor developed at NPS, the back side of the sensor has been left open, allowing for a measurement related to the pressure difference between the front and back of the sensor [3]–[4]. This design favors excitation of the bending mode in a dominant manner compared to the rocking mode. This pressure difference is related to the extra distance the sound wave needs to travel to impact the front and then the back of the sensor, and has been shown to have a cosine dependence on incident sound direction [3]. The positive half-cycle of a cosine repeats every 180 degrees, making the determination of quadrant of arrival impossible.

A two-sensor configuration was used by Wilmott [4] to resolve this ambiguity over a 120-degree detection range. More sensors can be combined to provide non-ambiguous 360-degree coverage. Such configurations require larger assemblies, complex electronics, difficult calibrations, and will consume more power.

A. BASIS FOR NEW SENSOR DESIGN

It is expected that closing the back of the sensor would have the effect of suppressing the directional dependence of the bending mode while presenting the rocking mode at a measurable amplitude with directionality. Without the interaction of sound with the back of the sensor, the pressure field amplitude will excite the pure bending mode with ideally no directional dependence [2]. The closure of the back will create a finite volume of air behind the senor wings that will act as a resistive mass, providing increased damping for the wing oscillations, lowering the amplitude of the bending mode signal compared to the open design. The rocking mode will be sensitive to the time difference of arrival between the two wings, providing directional sensitivity to the

output signal. When the sound field is incident normal to the plane of the sensor wings, there is no difference in arrival time between the wings and there will be no rocking mode excitation. As the incident direction moves away from the normal, the sound field will impact one wing first, starting the rocking mode, dominant on that side. The amplitude of the rocking should increase as the incident direction moves farther away from the normal axis, resulting in a sine dependence on arrival angle.

Acoustically, treating this enclosed cavity behind the sensor wings as a rigid-walled cavity and treating the bending wings as a driver oscillating at its mechanical resonance frequencies is straightforward. According to [7], if the wavelength of the sound in the fluid is much larger than all dimensions of the cavity, the cavity can be treated as a lumped acoustic element. Therefore, all acoustic equations reduce to the elementary case of the harmonic oscillator. The cavity dimensions are on the order of few millimeters in all directions. The frequencies of interest are 1100 Hz and 1460 Hz for this device. Assuming sound speed in air of 343 m/s, this results in wavelengths of 312 mm at 1100 Hz and 235 mm at 1460 Hz. Thus, we can treat the cavity as a lumped acoustic element for this analysis.

Simulation of the MEMS device performance with a closed air volume behind the sensor were performed in COMSOL Multiphysics. Figure 3 shows the sensor's frequency response at a 45-degree arrival angle from the normal plane. Note the prominence of a resonant peak at a lower frequency that appears at the 45-degree incident angle. Variations in simulation parameters, such as stiffness of the backing material behind the sensor, changed the relative magnitude of the rocking mode peak compared to the bending mode peak. However, with the back of the sensor closed, simulations always show the rocking mode more prominently than simulations with the back of the sensor open.

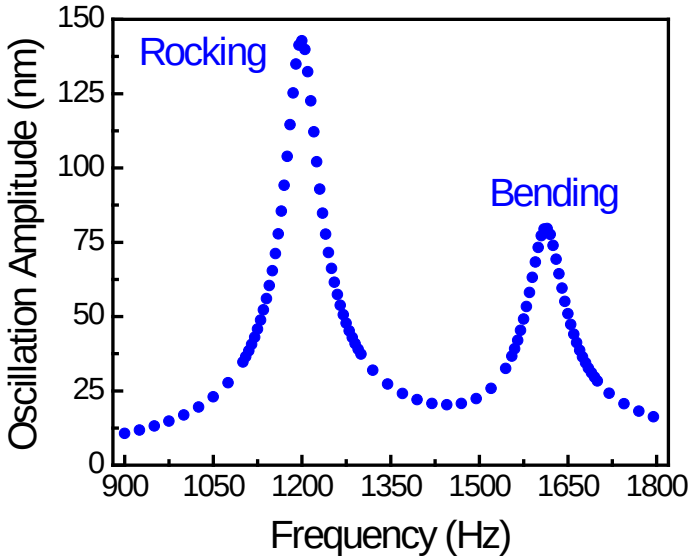

This figure shows the results of a COMSOL simulation of a MEMS sensor with an enclosed air volume behind it. The simulated sound source is a plane wave incident from 45 degrees off of the normal axis of the sensor. The sound pressure simulated at the sensor is 1 Pa. The rocking mode peak is near 1200 Hz and the bending mode resonant peak is near 1625 Hz.

Figure 3. COMSOL Simulation of MEMS Sensor With Back Side Enclosed, Frequency Sweep 900–1800 Hz

Figure 4 shows the sensor's simulated directional response at the bending frequency and rocking frequency. Note the relatively flat amplitude of the sensor response at the bending mode, which is consistent with Miles [2] analysis, as well as the sine dependence of the rocking mode frequency.

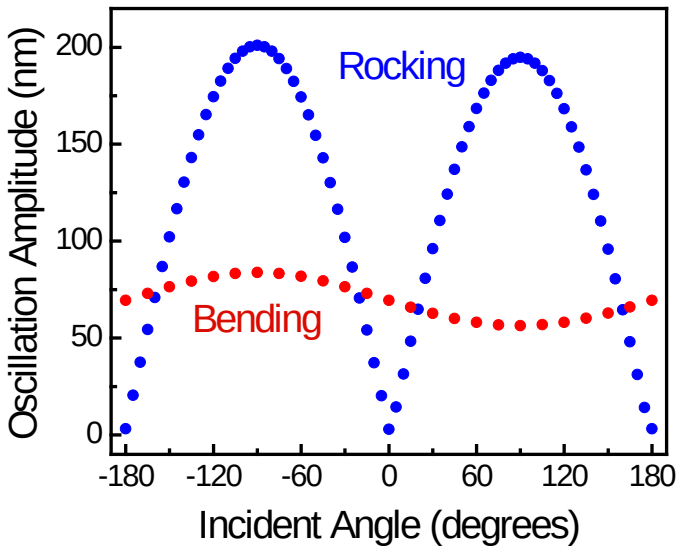

This figure shows the results of two COMSOL simulations of a MEMS sensor with an enclosed air volume behind it. The simulated sound source is a plane wave at a fixed location providing a sound pressure of 1 Pa. The sensor was rotated and the amplitude of the wing oscillations are shown here. The bending mode is relatively flat compared to the previous sensor design with the back side open. The rocking mode demonstrates the sine dependence expected from the rocking mode, as well as the asymmetric amplitude of oscillation based on side of arrival discussed by Miles [2]

Figure 4. COMSOL Simulation of MEMS Sensor With Back Side Enclosed, Rotation at Bending and Rocking Mode Frequencies

According to Miles [2], the large but finite stiffness of the bridge indicates that the resonant frequency of the bending mode is expected to be higher than that of the rocking mode. This is consistent with the frequency sweeps we have simulated that show the rocking mode at a lower frequency than the bending mode.

This design change requires a different approach to measuring the output of the MEMS device. Previous designs measured the combined capacitance of both wings and compared them to a reference capacitor consisting of fixed comb fingers built into the MEMS device [3]–[5]. This differential capacitance was fed into the MS3110 chip that outputs a voltage corresponding to the input. But according to Miles, the rocking mode responds to the difference between forces acting on the two wings and the bending mode only responds to the sum of the forces. Therefore, taking the difference between the two wing output signals should be sufficient to provide directional information about the incoming signal. However, the normal method of reading the signal discussed above does

not allow for measuring differences between the wings. In order to measure the difference between the wings' responses, we placed two sensors next to each other with one wing of each sensor wired to its own MS3110 chip, as shown in Figure 5. This allows each output to provide information about only one wing of the MEMS device, and can be used to measure the right wing on one chip and the left wing on the other. Since the sensors are very close to each other, the effect is the same as measuring both wings of the same sensor independently.

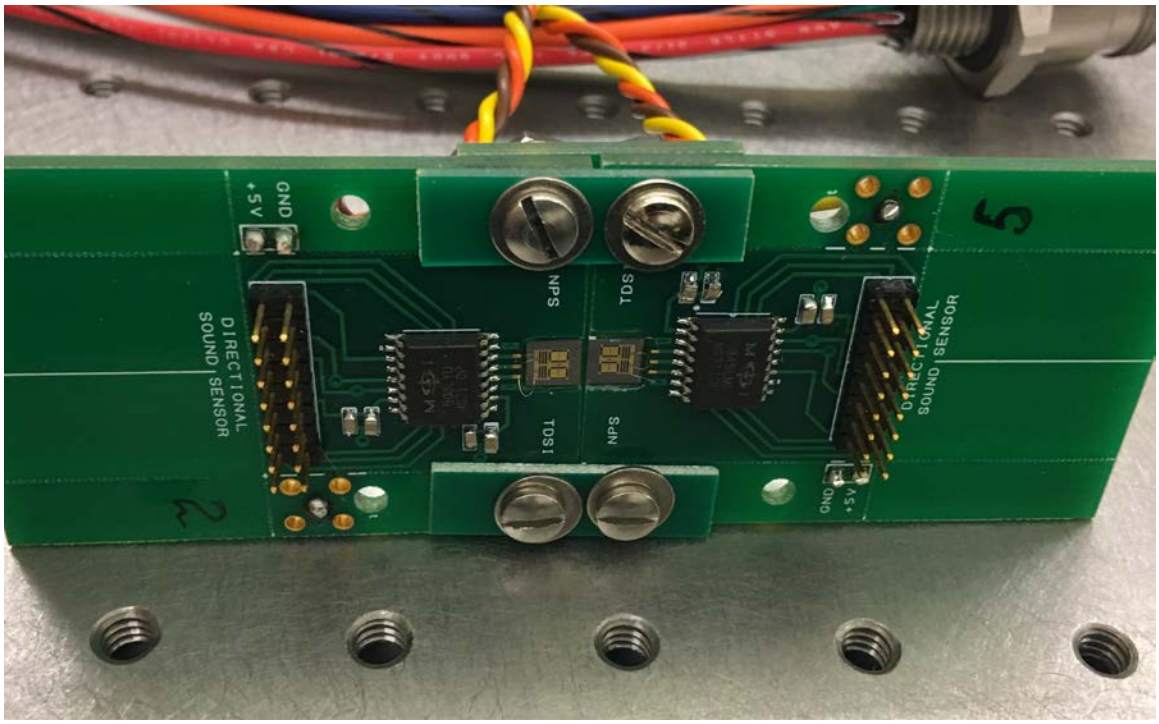

Figure 5. Two Sensors in Parallel with One Wing of Each Sensor Wired to an Independent MS3110 Chip

This arrangement complicates recording the data from acoustic testing. The SR865 lock-in amplifier used for testing only accepts one input at a time [8]. Therefore, two data runs for each test were performed to collect the response of each wing separately. One possible way to electronically read the difference between the wings in a single sensor is to connect the wings independently to the capacitive inputs of the MS3110, which would provide an output proportional to the difference between them.

This arrangement would eliminate the necessity of reference capacitors embedded in the sensor die, simplifying fabrication and retrieval of non-ambiguous directional response.

According to Miles [2], the amplitude of the natural modes is dependent on the time difference of arrival between the tympanal membranes of the fly. In his testing, he used a laser vibrometer to measure the amplitude of the fly ears' response to incident sound waves. He was interested in determining the source of the coupling between the eardrums. In the fly, the thorax creates a sealed air volume behind the eardrums. This is similar to the arrangement of the hearing organ in a cicada, which couples acoustic signals between the eardrums via the stiffness of this enclosed air volume. Miles identified that, in the *Ormia* fly, removing the front pair of legs would open the air volume behind the ear. If the stiffness of the enclosed air in the fly thorax were the transmission mechanism of the acoustic signal between the eardrums, then removing these legs would suppress the coupling between them. However, when he retested the eardrum motion after removing the legs, he found no change in the coupling, demonstrating that mechanical coupling via the intertympanal bridge was the source of the acoustic signal transmission. However, it does not necessarily preclude a different response altogether if the back side enclosure were completely removed. The open-back sensor design NPS has been using takes into account the extra travel distance for sound between the front of the sensor and the back of the sensor [4]. This addition of an additional phase term to the sound pressure amplitude function could account for the suppression of the rocking mode and the directional dependence of the bending mode in all previous NPS sensor designs.

The question of how a sound wave diffracting around a plate behaves very near the edge of the plate is a difficult one, with no straightforward general case answer readily available. Jebsen, for instance, investigated two models for sound field diffraction around an edge, but only analyzed the pressure field away from the edge [9]. His treatment would not necessarily hold along the tip of the wedge. As such, no complete analysis of why the response differs between closed back and open back is available. This is an area for future theoretical study.

B. TESTING THE NEW SENSOR DESIGN

1. Standard Data Collection Methods

There are two basic methods I used to record data from all of the sensors discussed in this paper.

a. Frequency Sweep

The SR865 Lock-in amplifier Aux Out port was used to provide 5 Vdc to power the readout electronics of the sensor. The SR865 sine output provides the electrical stimulus to the speaker via a HP467A power amplifier. The speaker used is a JL Audio 6 inch driver. The signal return from the sensor comes in to the 'A' port of the Lock-in via an SR560 Preamplifier filter. The speaker and the sensor are mounted in the NPS anechoic room approximately 3 meters apart, which is in the far field for 1500 Hz in air. The component arrangement is schematically illustrated in Figure 6. The sweep setting for the Lock-in is set for the desired start and stop frequencies. The step size defaults to 0.16 second. When the SR865 performs a sweep, the time axis progresses until the stop frequency is reached, and then it pauses time to retain your data on the screen. Additionally, the save feature records screen shots and data values limited to the information on the screen at the time the save is executed. Therefore, an appropriate setup for the tests requires 10 seconds/division on the time axis and 100 seconds total sweep time.

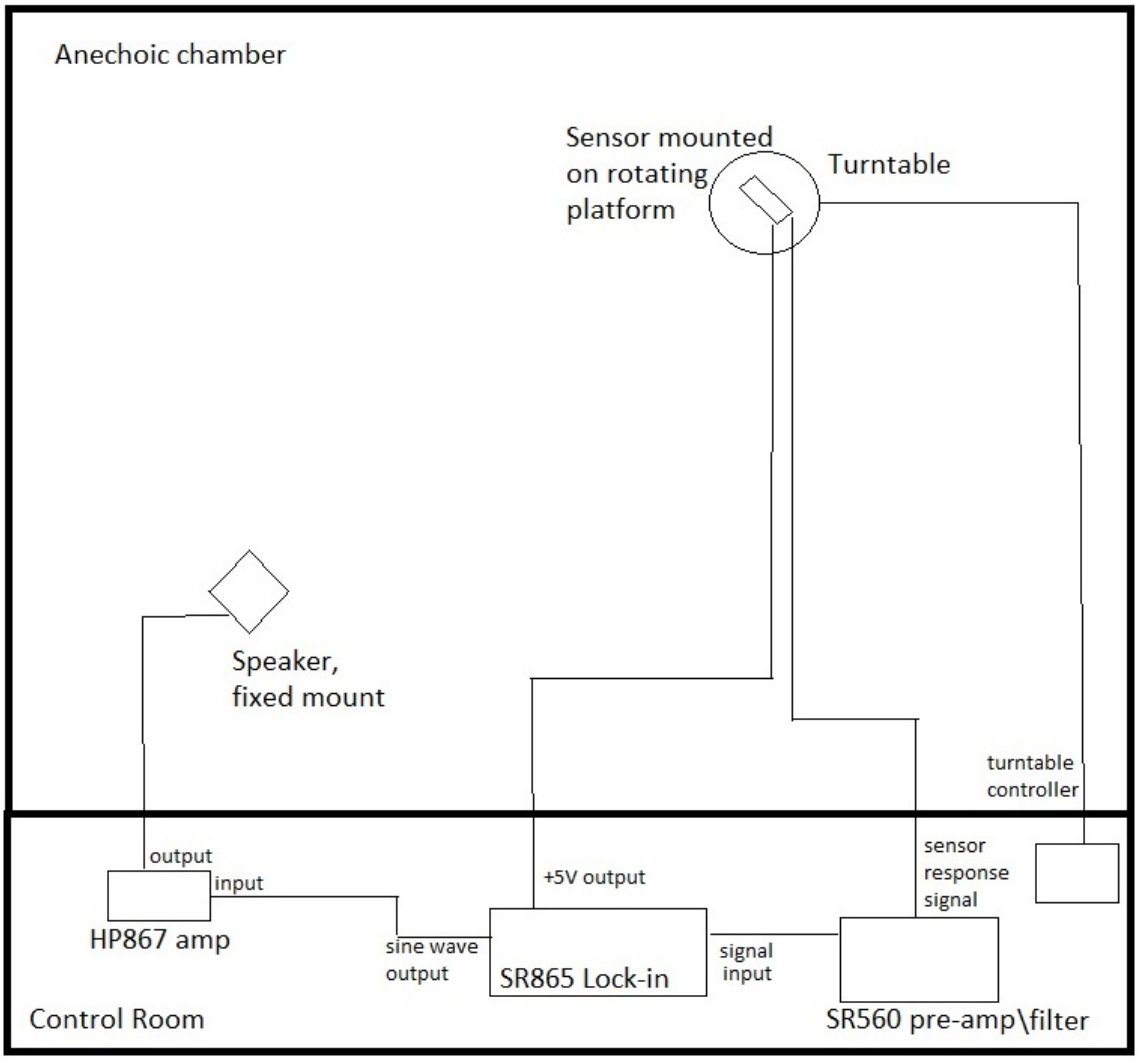

Figure 6. Block Diagram of the Anechoic Room Test Equipment Setup

b. Rotation test

All equipment is connected as above, with the sensor mounted on a turntable connected to a B&K Type 5997 turntable controller. The 5997 was set to 99.3 seconds/ revolution to be consistent with the 100 seconds per sweep setting from above. Each rotation begins with the sensor facing directly away from the speaker, and the rotation direction remains constant throughout all testing. When using the SR865 to check for a response at a single frequency, I found it necessary to set a sweep running from, for instance, 1459.9 to 1460.1 Hz over 100 seconds. This is not a significant enough change

in frequency to affect the quality of the output and it still causes the time axis to pause at the end of the sweep so that the user can record the correct data. If the start and stop frequencies are the same value, the sweep function never identifies that the appropriate amount of time has elapsed and the sweep continues indefinitely.

2. Experimental Results for Open Back Dual Parallel Sensor Arrangement

For the experimental setup, we arranged the sensors on adjacent PCBs as shown in Figure 5. Open back testing was performed first to verify sensor response. A frequency sweep was performed to confirm the bending mode resonant frequency at 1490 Hz and then a rotation test at that frequency to confirm the expected cosine shape of the bending mode seen in Wilmott [4]. Figure 7 shows the frequency sweep results for the open back sensor configuration with the sound incident normal to the sensor and Figure 8 shows the frequency response with the sound incident 45 degrees from the normal to the sensor. The directional response of the open back arrangement to the bending mode frequency is shown in Figure 9. Lock-in and pre-amp settings for open back dual sensor data sets are given in Appendix A.

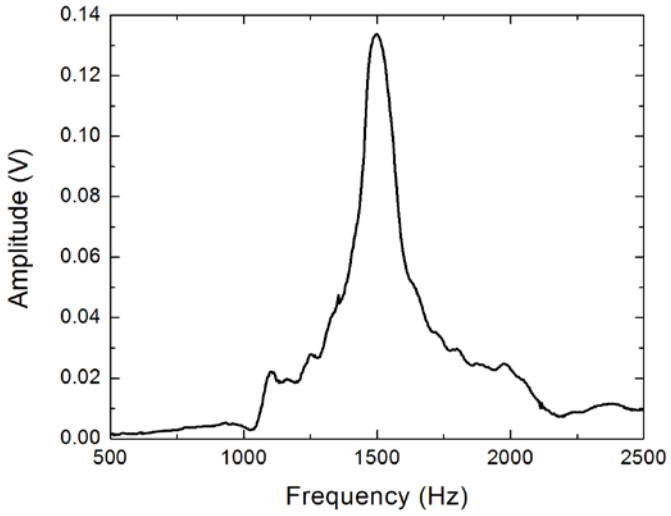

Figure 7. Open Back Sensor, 500–2500 Hz Frequency Sweep, Normal Incidence, Sound Pressure at Sensor of 31.1 mPa

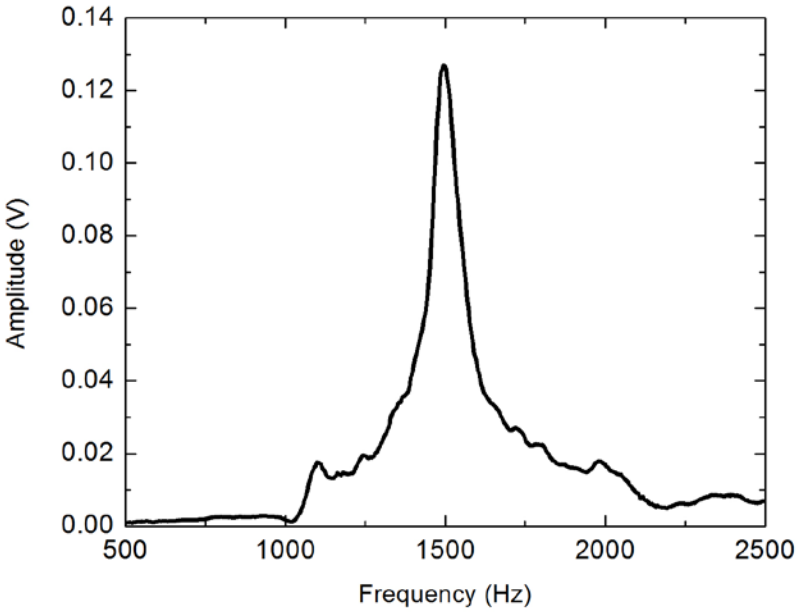

Figure 8. Open Back Sensor, 500–2500 Hz, 45 Degree From Normal, Sound Pressure at Sensor of 31.1 mPa

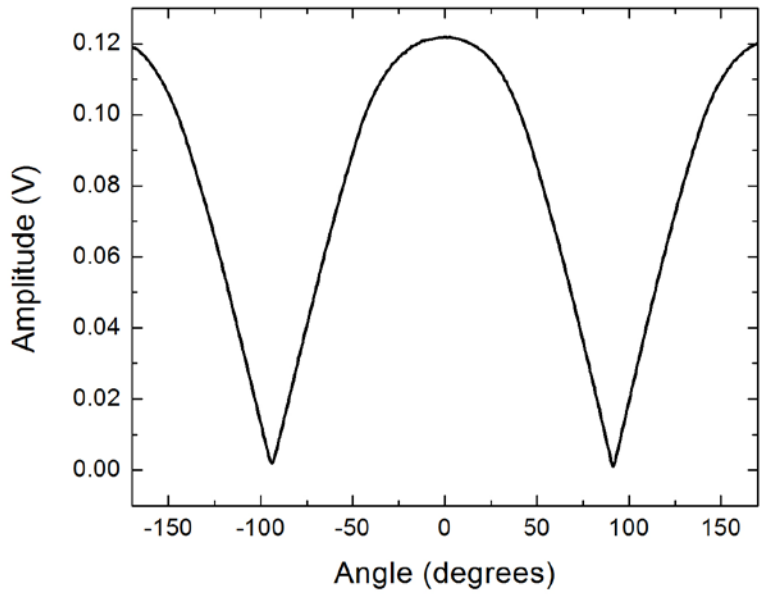

Figure 9. Open Back Sensor, Directional Response at 1460 Hz (bending mode), Sound Pressure at Sensor of 31.1 mPa

3. Experimental Results for Closed Back Dual Parallel Sensor Arrangement

a. Sensor issues

After the open back verification was complete, the back side of the sensor cavity was closed by attaching a remnant piece of PCB material, as shown in Figure 10. Both sensors were retested with a frequency sweep and rotation. Unfortunately, coincident with the installation of the PCB piece to close the back, one of the chips failed electronically and will no longer provide a sensible readout. Thus, all data with the back closed is from the remaining working sensor. Based on this result, only the results from the open back testing for this working sensor are shown in Figures 7, 8 and 9 as well.

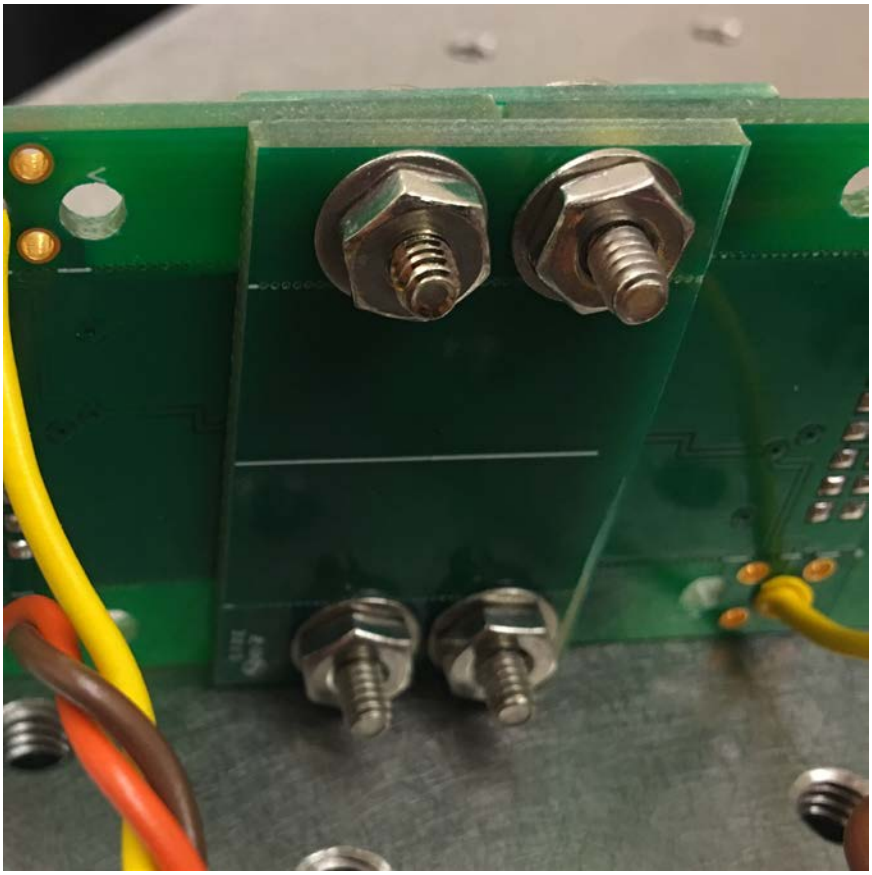

Figure 10. Closing the Back of the Dual Parallel Sensor Assembly Using a Piece of PCB.

b. Noise issues

We were able to isolate and remove a significant noise source during the performance of this testing. Initial wire harness arrangement included a common ground lead between the two separate MS3110 chips. However, this introduces electronic noise in the 3 kHz range due to the inability to perfectly synchronize the onboard clocks of the two MS3110 chips. Disconnecting these two ground leads improved the signal quality and removed beating that we were experiencing in the output. The difference between the output signals with and without ground connection is shown in Figure 11.

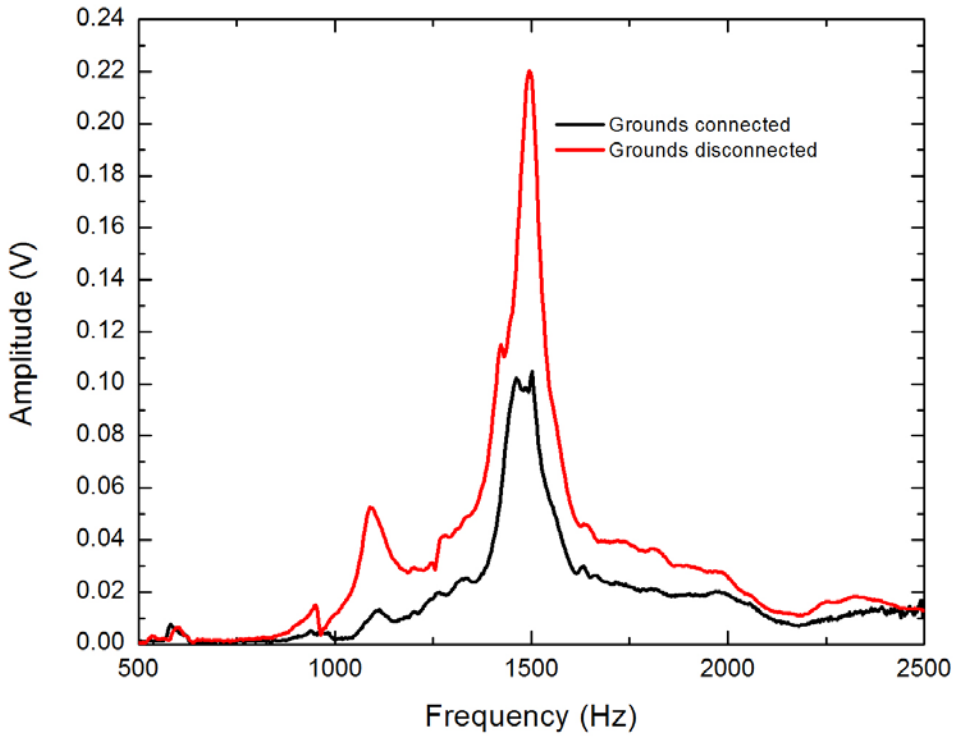

The 2.7 kHz electronic noise originating from the clock mismatch between the two MS3110 chips resulted in a beating with the resonant mechanical response of the sensor, leading to a notch in the resonant peak and overall reduced signal output.

Figure 11. Effect of Separate Ground of the Parallel Sensor Array on the Sensor Frequency Response

c. Frequency Sweep and Rotation Results

Even with the noise due to the ground connection removed, it was found that the second sensor was not operational, and took as much data as possible with the working sensor. Frequency sweeps were taken with the sensor facing the speaker, and at a 45-degree tilt on both sides of normal incidence. As shown in Figures 12 and 13, the bending response at 1460 Hz is still evident as with the open back testing. Measurements were done setting the amplifier gain of the speaker to twice the value used for the back side open sweeps. Additionally, the signal from the sensor was passed through an SR560 preamplifier set to 10X gain. These effects combine for a 20 times increase in output magnitude for closed back compared to open back, but the measured amplitude at the resonant peak is only about 2 times higher with the backside closed. The overall effect of closing the back drives the signal around 10 times lower than that of the open back sensor. A reduction in vibration amplitude of the sensor response is expected with the back side of the sensor enclosed due to the stiffness of the air in the cavity and lack of interaction of sound from the back. The enhanced peak at 1100 Hz in the 45-degree tilt data in Figure 13 is the rocking mode resonant response. Lock-in and pre-amp settings used for closed back dual sensor data sets are given in Appendix A, while MS3110 EEPROM settings are given in Appendix C.

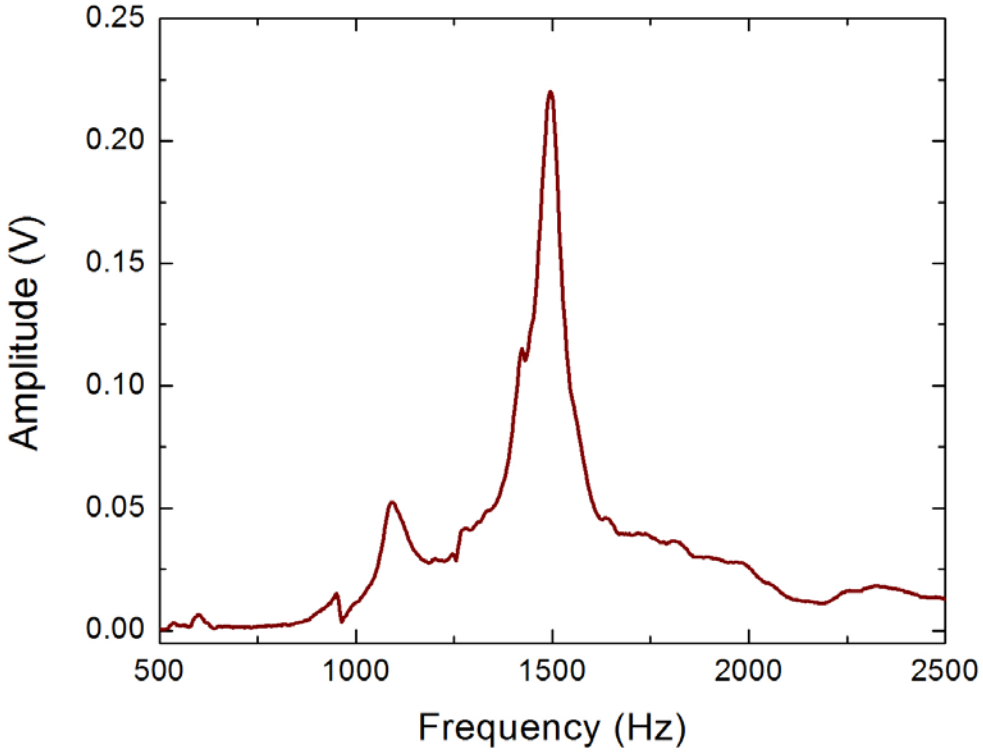

Figure 12. Closed Back Sensor, Frequency Sweep 500–2500 Hz, Normal Incidence, Sound Pressure at Sensor of 59.7 mPa

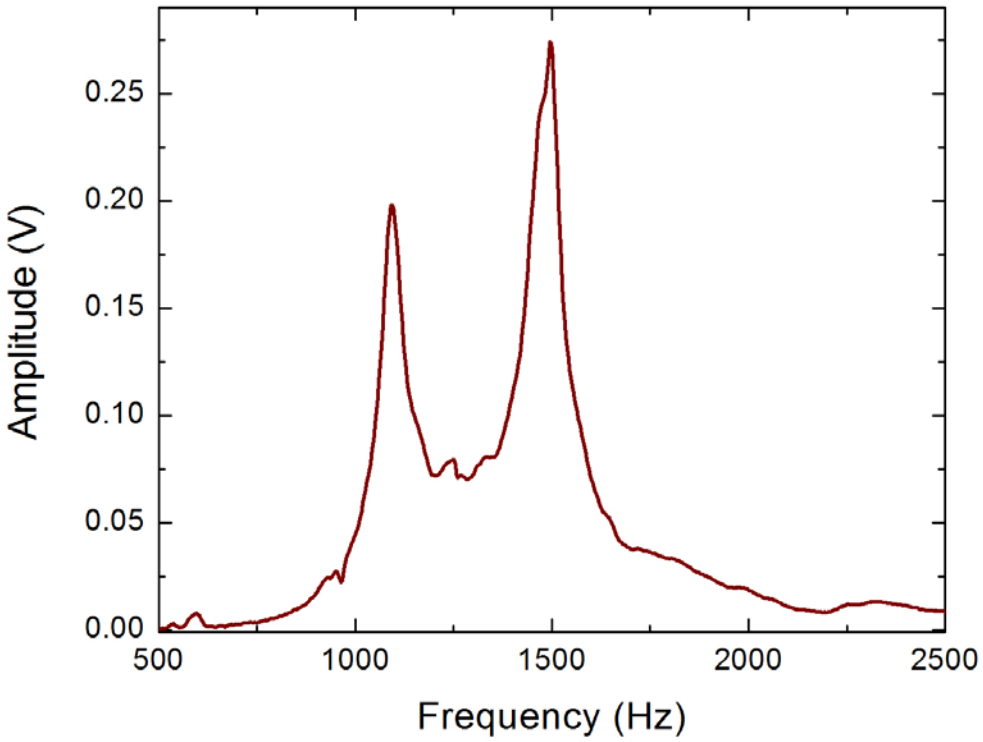

Figure 13. Closed Back Sensor, Frequency Sweep 500–2500 Hz, 45 Degrees Offset From Normal, Sound Pressure at Sensor of 59.7 mPa (About 69 dB).

Rotation testing results at the bending frequency, 1490 Hz, and the rocking frequency, 1100 Hz, are shown in Figure 14. Noteworthy features of the bending response include the relatively flat response with respect to direction. This is consistent with the Miles results previously discussed [2]. At the rocking resonance, a measureable output was observed for the first time with a sine response with respect to direction, akin to what Miles reported for the fly. Importantly, it is evident that the rectified sine wave is asymmetric, with one side higher than the other. This is consistent with Miles' findings that the peak amplitude of the fly ear oscillation was larger on the side that the sound was coming from due to coupling between the rocking and bending modes [2]. It was expected that the second sensor, if it were working, would show the same asymmetry between the two opposing wings. For the final analysis, we have reflected the working sensor output around the normal axis, based on this expectation.

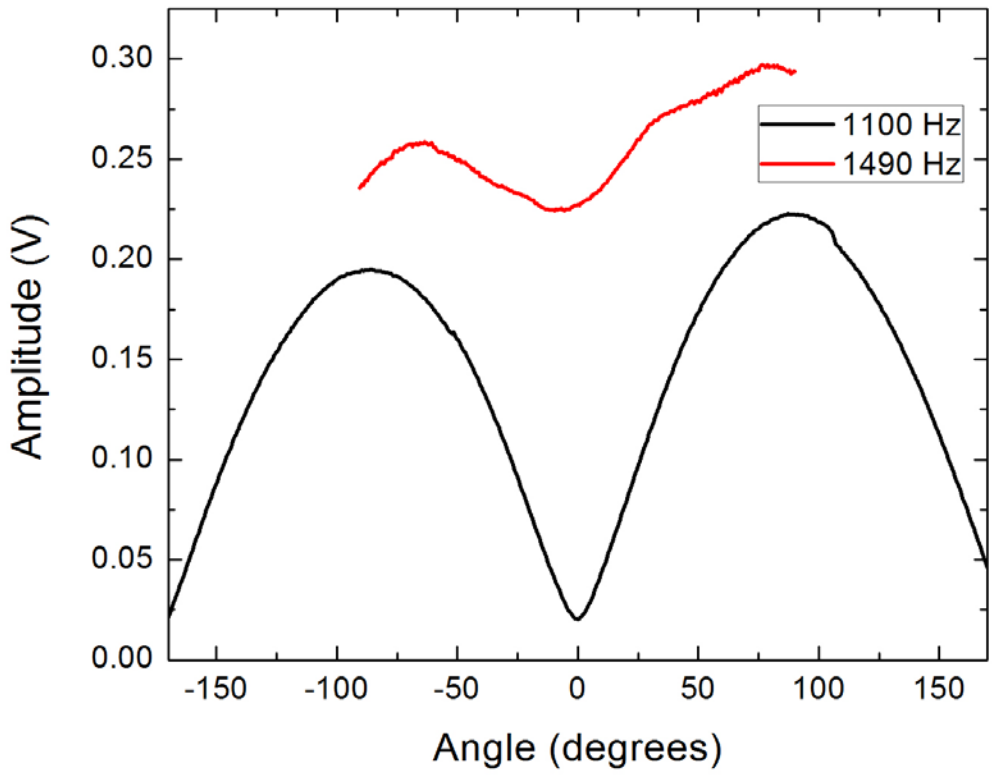

Figure 14. Closed Back Sensor Rotation Test at 1490 Hz (Bending Mode) and 1100 Hz (Rocking Mode).

d. Sensitivity

To determine the sensitivity of the sensor in the closed back arrangement, the bending mode response amplitude was measured at normal incidence at four speaker voltage settings and compared those values to the response of a reference microphone at the same speaker output. The sensitivity of the B & K Type 4138 microphone is given as 1 mV/Pa in [10]. The microphone was connected through a Listen, Inc. Sound Connect microphone power supply set to +60dB gain, yielding a sensitivity of 1 V/Pa for the system. Table 1 shows the measured input voltages to the speaker, and the responses of the microphone and the closed back sensor, accounting for the 10x gain applied to the closed back sensor's signal by the SR560 preamp. The sensitivity of the closed back sensor is thus shown to be 0.197 V/Pa.

Table 1. Sensitivity Measurement of the MEMS Sensor with Back of Sensor Closed

Speaker output (V_{rms})	Ref Mic (mV)	Sound Pressure at sensor (mPa)	MEMS closed back sensor output (mV)	MEMS closed back sensitivity at 1460 Hz (V/Pa)
2	13.5	13.5	2.61	0.193
4	25.4	25.4	5.02	0.198
10	59.7	59.7	11.78	0.197
20	114.6	114.6	22.55	0.197

e. Directionality

Direction finding based on exploiting the rocking mode involves the simple difference in amplitude between the signals given by the two wings. The sensor output was normalized to a maximum value of 1, the output of the working sensor was subtracted from its reflection, and achieved the linear response shown in Figure 15.

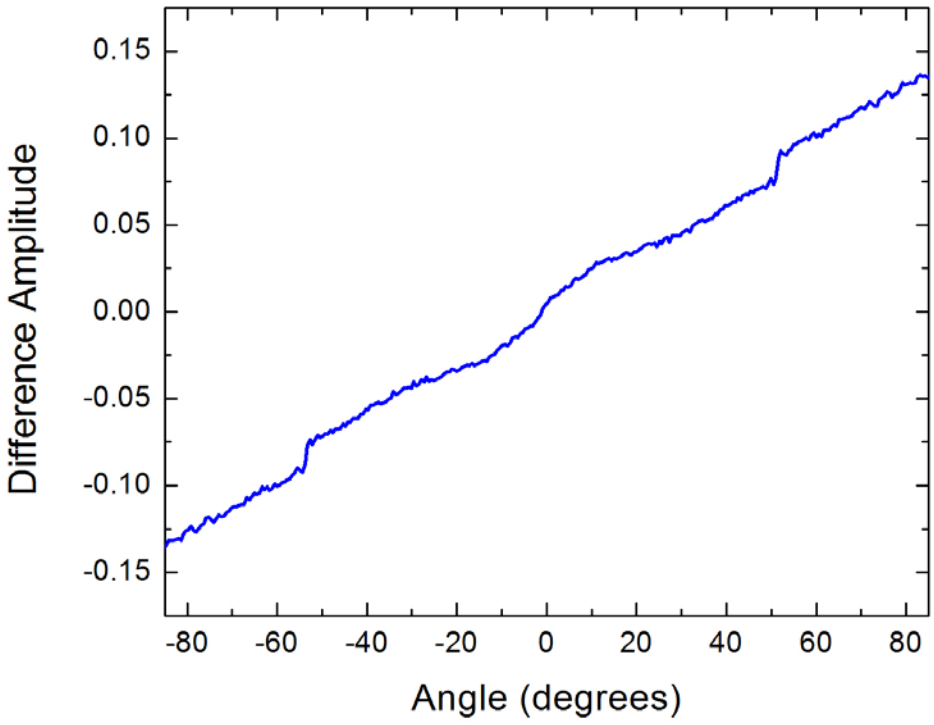

Figure 15. Difference Between Normalized Signal Amplitude of Two Wings When Oscillating at the Rocking Mode.

This result demonstrates that single-sensor directionality is achieved by a proper exploitation of the rocking mode with the back side of the sensor closed. The difference in individual wing outputs found to be linear from -90 to 90 degrees. This would represent an improvement on the two-sensor array demonstrated by Wilmott [4], which provided coverage over a 120-degree range due to the use of 30-degree canted angle. The initial results show that a single sensor operating at the rocking mode can be used for unambiguously determining the direction of arrival.

III. UNDERWATER SENSOR AND HOUSING DESIGN

In order to probe the feasibility of adopting MEMS directional sound sensor described earlier for underwater applications, a new sensor design and housing assembly needs to be created. Several material considerations went into the selection and design of parts for this housing.

A. SELECTING MATERIALS FOR THE SENSOR HOUSING

1. Case Material

The case must be acoustically transparent at the wavelength of interest in the water.

a. Sound speed in Flexane 80

Flexane 80 Liquid 2-part urethane compound was selected for the sensor case. The sound speed and specific acoustic impedance of the urethane was measured for use in subsequent analysis. A disk of the Flexane 80 was prepared with a diameter of 4 inches and average thickness of 3 mm. An Olympus Panametrics NDT Model 5072PR with the longitudinal transducer A107S hooked up to a Tektronix DPO 71254 oscilloscope was used to measure the sound speed in the sample. The sound speed measured by this method was c = 2400 +/- 25 m/sec. From the technical data provided by Devcon, [11] the specific volume of Flexane 80 is 26.5 in^3/lb and density of $\rho = 1045$ kg/m^3. Therefore, the characteristic acoustic impedance of Flexane 80 is

$$r = \rho \times c = 2.51 \times 10^6 \, Pa \cdot s / m$$

b. Acoustic properties of the case in water

At the frequencies examined for this underwater application, wavelengths are on the order of 10 meters. The urethane case we have created for this application is 0.1 inches (0.254 cm) thick, much less than the length scale of the wavelength. From [7], the transmission coefficient for a sound wave through two boundaries reduces to

$$T = \frac{(4r_3 r_1)}{(r_1 + r_3)^2}$$

when the intermediate layer is thin compared to a wavelength and

$r_2 \sin(k_2 L) \ll 1$ and $\cos(k_2 L) \approx 1$.

In these relationships, r_1 and r_3 are the specific acoustic impedance of the materials on either side of the thin barrier, k is the wave number in the barrier, and L is the barrier thickness. For this housing, the underwater test frequency band

$$k_2 L = \frac{2\pi fL}{c}$$

is on the order of 0.001, where c is the sound speed in the barrier, and f is the test frequency. This kL value is small enough to justify small angle approximations for the sine and cosine relationships stated above, meeting the requirements to acoustically ignore the urethane barrier layer between water and the fill fluid. For fresh water used in the acoustic test tank at NPS, the specific impedance is $r_1 = 1.48 \times 10^6$ Pa * s / m. As discussed in Section III.A.2, silicon oil will be used as the fill fluid, and it has specific impedance $r_3 = 9.41 \times 10^5$ Pa * s / m [12]. The resultant transmission coefficient is T = 0.95.

c. Acoustic properties of the case in air

Part of the characterization of the new sensor will involve testing it in air prior to submerging it. Therefore, it is instructive to analyze the transmission coefficient for sound waves across the urethane barrier going from air to air. According to [7], the transmission coefficient for sound starting and ending in the same type of fluid (air in this case), with a thin barrier of a relatively higher characteristic acoustic impedance, provided the frequency is not too high and the wall is not too thick, reduces to

$$T = \left(\frac{2r_1}{k_2 L r_2}\right)^2.$$

For air, $r_1 = 415$ Pa s/m. At the frequency band used for air testing for this sensor, $k_2L = 0.005$. This yields a transmission coefficient of $T = 3.4 \times 10^{-3}$.

2. Fill Fluid

The sensor and the PCB where it is mounted must be in a non-conductive medium to prevent shorting the circuitry employed in measuring the amplitude of oscillating

wings. We have selected PSF-2cSt silicon fluid as the fill medium due to its non-conductive properties, low viscosity, and sound speed similar to that of water.

The sensor wings must still be able to oscillate freely upon an incident sound wave. The existing air sensor was constructed with a 2 micron gap between the comb fingers and the substrate, and it was used first to check for wing movement in the silicon oil. The sensor was immersed in a dish of the oil, a speaker was mounted above it to provide a sound stimulus, and a laser vibrometer was placed above it to probe wing motion.

Initially, no wing motion was detected due to the stricture of the comb fingers to the substrate by the oil. When the sensor was removed from the dish and inspected under a microscope, it was noted that residual oil had permanently bound combs on the wings with that of the substrate. This information indicated the need for increased spacing between the comb fingers and the substrate greater than the 2 microns used in previous generations of air sensors, and was incorporated into the design of the water-based sensor. This result also shows that, once the sensor has been placed in the housing in the oil, it cannot be removed without permanent negative consequences. In order to test this idea, another sensor was prepared by cutting away the comb fingers from one of the wings in an effort to reduce the likelihood that the oil would seize the sensor to the substrate. We confirmed with the laser vibrometer that the wing with no comb fingers oscillated freely under sound stimulus while immersed in the silicon oil. Since the sensors cannot be removed from the oil once submerged, the electrical cabling leaving the housing must be able to support programming the MS3110 chip as well as powering and reading the sensor output. Since programming the chip requires a 16 pin ribbon cable directly connected to the programming board, this has traditionally been performed with a dedicated cable on the lab bench whereas sensor response readout in the anechoic room or in the field can be done with a comparatively simple three wire connector. For the underwater sensor, both operating modes, programming and testing, must be performed with a single electrical fitting.

B. BUILDING THE SENSOR HOUSING

1. Constructing the Urethane Case

The housing for the sensor was created out of a mold designed and constructed at NPS. The mold, shown in Figure 16, was machined out of Delrin, chosen because it is easily machined, strong, and tends to release urethane molds well [13]. The housing is cylindrical with a hemisphere end cap, ensuring uniform thickness and minimal effect on sound transmission due to shape.

Figure 16. Delrin Mold for Sensor Housing.

2. Constructing the Sensor Mount and Closure Head

The sensor mount and closure head were printed using additive manufacturing processes available on site at NPS. The selected density of the printed filament material is sufficient to limit water penetration to 1% total weight change after 24 hours submerged. This is satisfactory based on the comparatively short test time that the sensor housing will be exposed to water. We would recommend that long term installations of this design

should be constructed of aluminum or brass. The closure backing ring was machined out of aluminum with an O-ring groove between the aluminum piece and the PCB mount. The finished PCB mount is shown in Figure 17. The complete sensor housing is shown in Figures 18 and 19.

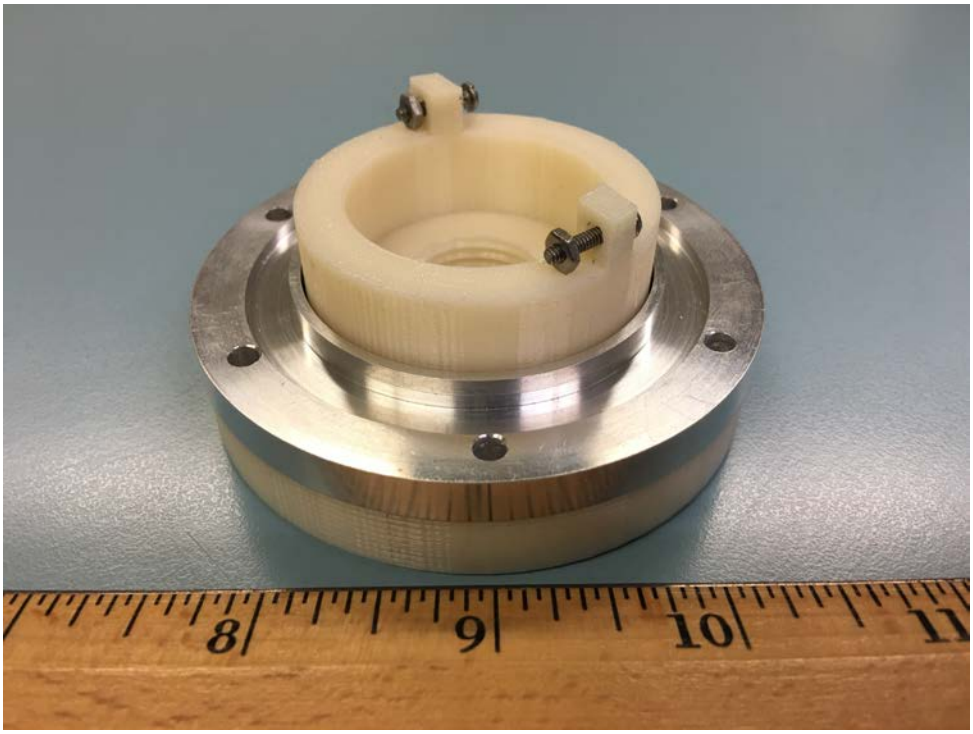

Figure 17. 3D Printed PCB Mount and Aluminum Backing Ring.

From left to right, the components shown here are (1) the finished Flexane 80 urethane shell, (2) the 3D printed backing ring, and (3) the 3D printed PCB mount and aluminum closure ring.

Figure 18. Components of the Underwater Sensor Housing.

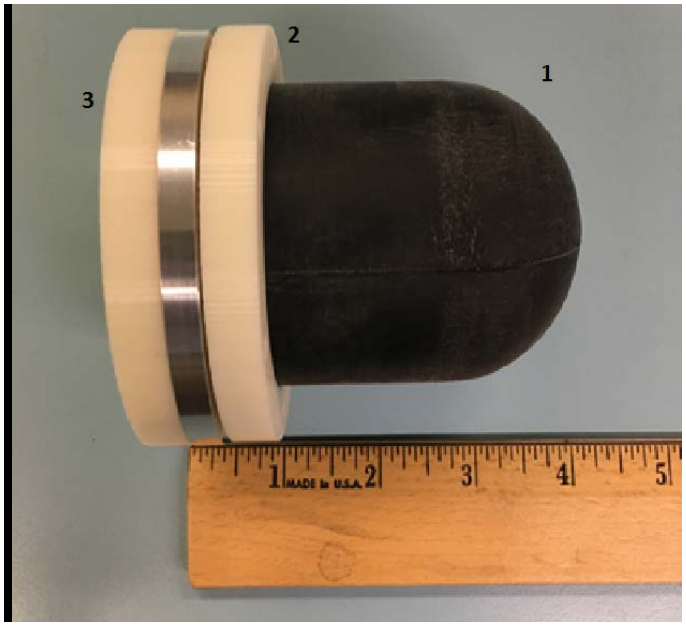

The components shown are (1) the Flexane 80 urethane shell, (2) the 3D printed PCB mount, and (3) the 3D printed PCB mount and aluminum closure ring.

Figure 19. Assembled Underwater Sensor Housing.

3. Electrical Connection to the PCB

The electrical connection selected was a 12 pole mini-link receptacle produced by Remke Industries, shown in Figure 20, selected because it screws directly into the closure head, creating an inherently watertight seal with the included O-ring. Additionally, it contains enough wires to both program the MS3110 chip and operate the sensor.

Figure 20. Remke Industries 12 Pole Mini-Link Connector, Part Number 112Q0010M1.

This is necessary since, as stated above, the sensor cannot be removed from the silicon oil without risking permanent stricture of the comb fingers to the substrate. Therefore, the sensor must be electrically connected to the closure head, then placed into the oil filled housing, and only then programmed, electrically balanced, and prepared for use.

C. DESIGN AND FABRICATION OF THE UNDERWATER SENSOR

The sensor design was completed using COMSOL and laid out using MEMSPRO software. The design used is shown in Figures 21–22. Due to the increased feature size of the wing necessary to achieve the desired underwater resonant frequency performance, we chose to use a single wing design to fit onto the existing PCBs. This design choice limits performance to a single resonant mode with a cosine dependent directionality along with the accompanying left-right arrival ambiguity. Future designs could take advantage of the 2 sensor assembly described in Wilmott [4] or test the closed back performance of the underwater sensor with two wings, as discussed above. Possible complications of a single wing design include limited sensitivity to longer wavelength sound waves. Miles [2] posited that the *Ormia* fly is able to successfully DF such a long wavelength, compared to the size of its hearing system, because of the mechanical coupling between the ear drums. Removing the second ear drum might either reduce the sensitivity of the sensor to the longer wavelengths we hope to exploit, or limit our ability to successfully DF the signal. However, all previous versions of the MEMS sensor have only exploited a single resonant mode, rather than mixing the bending and rocking modes like the fly, and we have been able to overcome this deficit to successfully DF a sound signal.

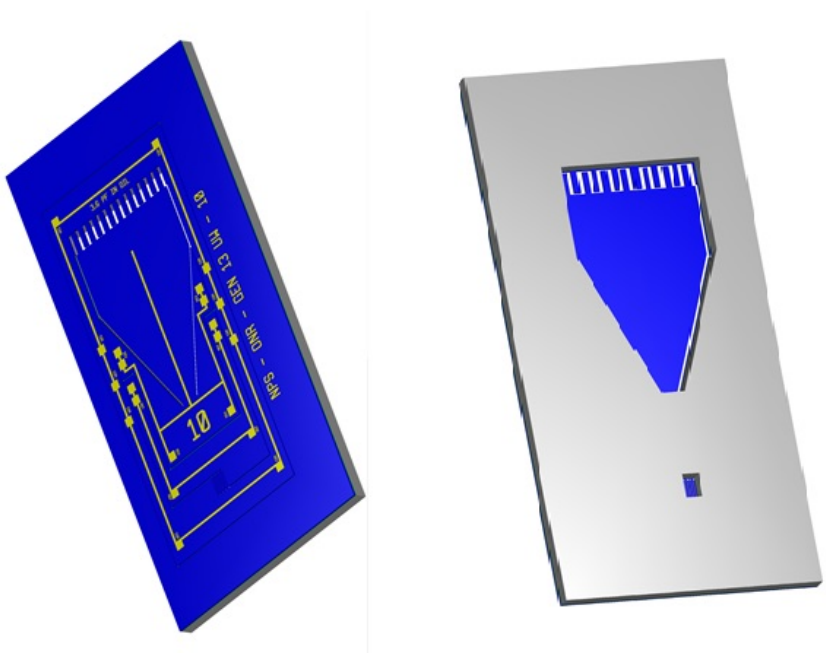

Figure 21. Top and Bottom View of Underwater Acoustic Sensor Design, Produced from MEMS PRO L-edit.

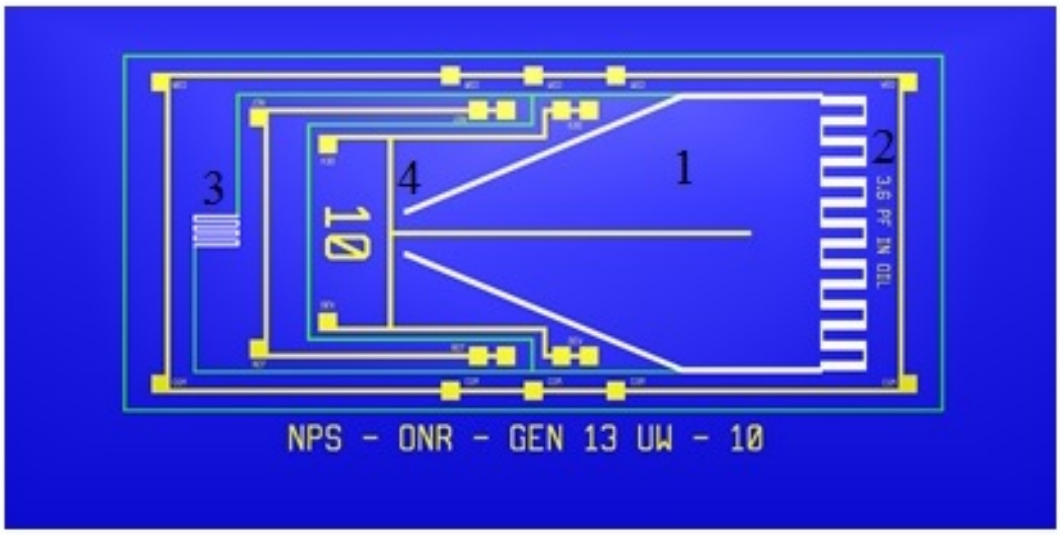

Features indicated are (1) the oscillating wing simulating the fly eardrum, (2) the interdigitated comb finger capacitor for readout, (3) the fixed reference capacitor for differential capacitance readout, and (4) the fixed connection point representing the intertympanal bridge of the fly ear.

Figure 22. Detail View of the Underwater Acoustic Sensor Design, Produced in MEMS PRO L-Edit.

The sensors were fabricated at MEMSCAP foundry using traditional SOIMUMPS architecture [6]. Sensors with both 5 microns and 10 microns gap size between the comb fingers were fabricated. In future testing, the differences in output and performance based on these variations will be probed, assisting in optimizing future sensor designs. This design pushed the limits of the commercially available manufacturing processes for this type of device due to the feature size and layer thickness required to achieve the desired underwater resonant response frequency. Further modifications to the design should be possible using newly available on-site clean room facilities in the future.

Simulations of the sensor performance were carried out in COMSOL Multi-Physics [14]. Figure 23 shows the basic geometry used in the finite element simulations. Figure 24 shows the frequency response of the sensor design in water and Figure 25 shows the directional response at the resonant frequency. Note that the simulated sensor response has a sharp resonant peak and a cosine dependence on direction that we would expect from the bending mode resonance of an open backed design described earlier. No rocking mode resonant peak is expected to appear with this sensor due to the single wing design.

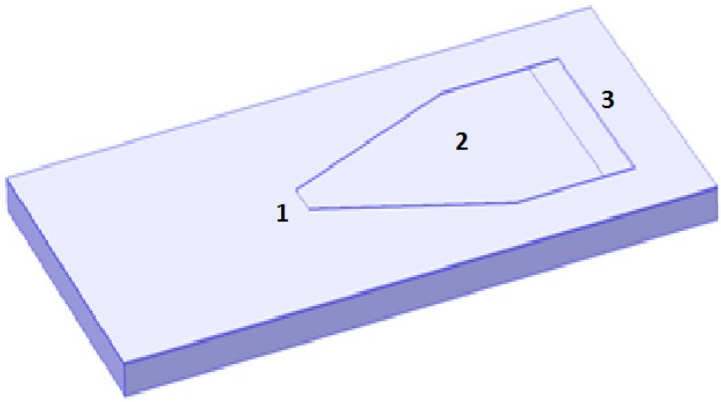

This image shows the fixed point (1) representing the connection to the substrate, (2) the oscillating wing representing the eardrum, and (3) the comb finger capacitors.

Figure 23. Basic Geometry of the COMSOL Simulation of the Underwater MEMS Sensor for Testing Frequency Response.

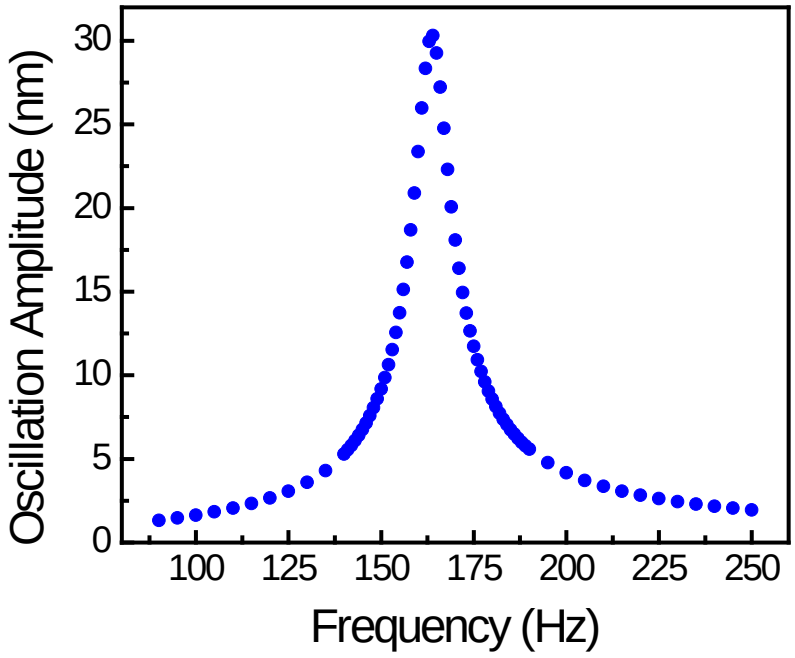

The expected frequency peak is around 160 Hz.

Figure 24. COMSOL Simulation of the Underwater MEMS Sensor's Frequency Response.

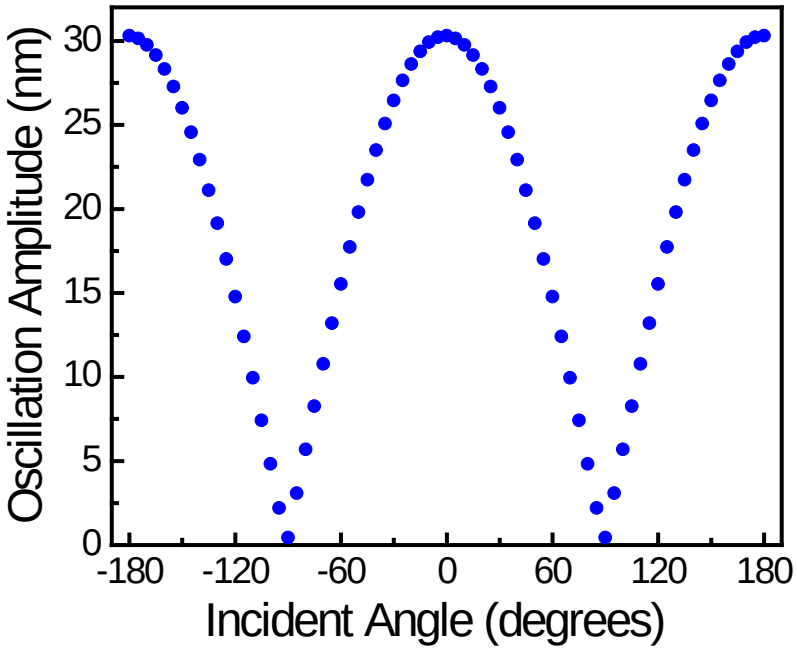

Figure 25. COMSOL Simulation of the Underwater Sensor's Directional Response at the Resonant Frequency of 160 Hz.

The underwater MEMS DF acoustic sensor has been designed and fabricated. The sensor characteristics have been modeled in COMSOL Multiphysics with results showing expected performance characteristics. An appropriate housing to contain the sensor for underwater testing has been designed, fabricated, and assembled.

IV. EXPERIMENTAL SETUP AND RESULTS

A. PROGRAMMING AND BALANCING THE MS3110

1. Cabling

Setup for testing of the new sensor required constructing a wiring harness adapter to connect the 16 pin connector on PCB to the 12 wire plug on the housing. In order to meet the requirement that the sensor must be programmed and read after the housing is filled with oil and sealed, it was desirable to make a single cable to connect the sensor's electrical connector to either the MS3110 programming board or equipment to read the output signal. Previous sensor designs have used a 16 pin ribbon cable to connect to the programming board and a separate wire harness soldered on to contact pads on the PCB to connect to the oscilloscope or lock-in amplifier for readout. We attempted to integrate both functions into a single 3 meter cable as shown in Figure 26.

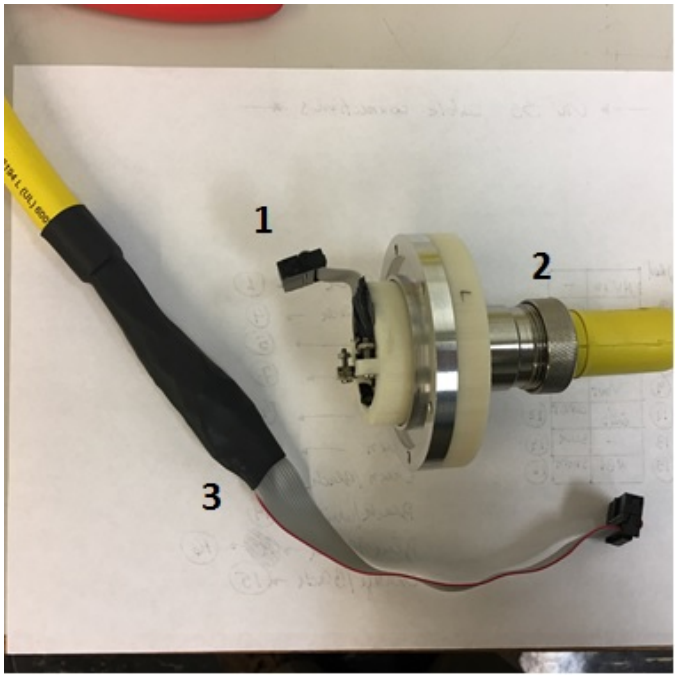

This figure shows (1) the ribbon cable spliced into the Mini-Link connector at the PCB mount, (2) the Mini-Link cable plugged in to the connector mounted in the housing closure, (3) and the ribbon cable spliced onto the end of the 3 meter transmission cable.

Figure 26. 12 pin Mini-Link Cable Spliced Into 16 Pin Ribbon Cable at Both Ends.

Once the cable adapters were wired appropriately to connect the sensor to the housing's electrical connecter and to connect the housing output to the programming board, a sensor was mounted to a PCB, as shown in Figures 27 and 28, and attached to the mount as shown in Figure 29.

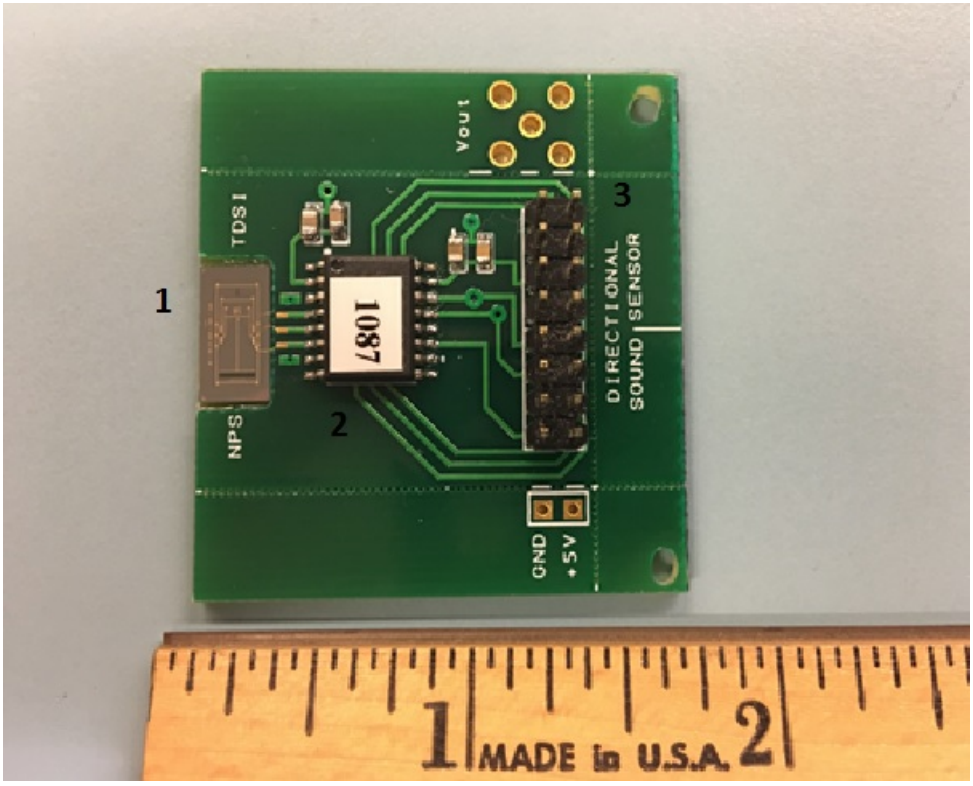

This figure shows (1) the underwater sensor mounted to the PCB, (2) the MS3110 chip, and (3) the 16 pin ribbon cable connector used for programming and operating the sensor.

Figure 27. Underwater Sensor Mounted to the PCB.

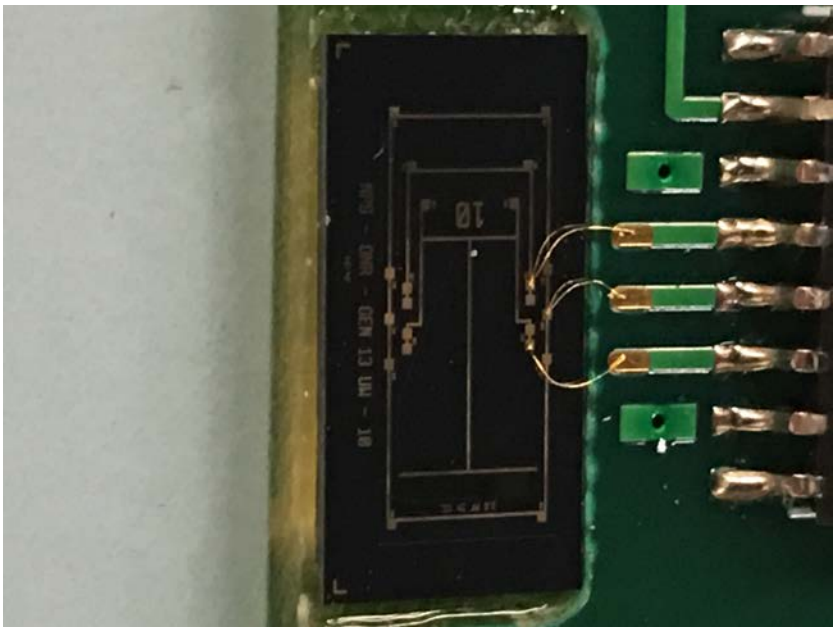

Figure 28. Close-up of Underwater Sensor Mounted to PCB, Detail View of Wire Bonding.

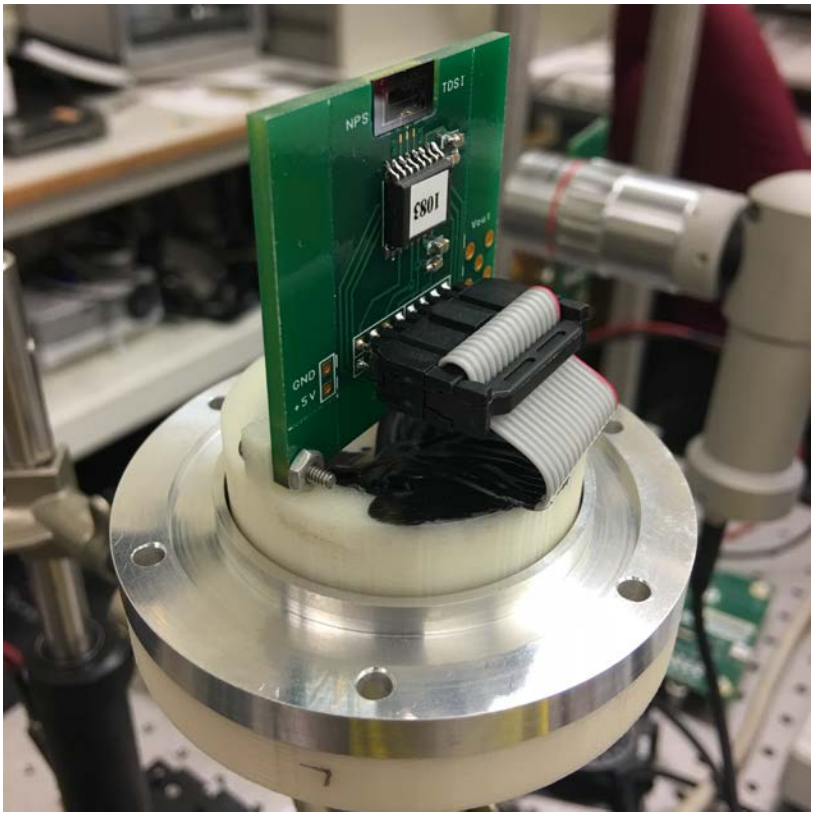

Figure 29. Underwater Sensor PCB Mounted to Case.

2. Programming the MS3110

When attempting to program the MS3110 chip, the digital signal to send commands back and forth between the chip and the programming board became garbled over the long transmission line at the relatively high clock frequency of the programming board. The control software was unable to successfully write to the EEPROM or report what the stored values in the EEPROM actually were. Continuity checks along the cable confirmed that the spliced connections were sound, so a shorter cable connected directly to the PCB was tested, bypassing the connector we built into the sensor housing. It was able to successfully communicate with and program the chip that way, but left the question of how to program the chip after the housing was assembled. Two versions of the external cable were created, one shorter cable (30 cm) with all leads connected to the 16 pin ribbon cable to allow for programming, and one longer cable (3 m) that terminates with three leads providing +5 V power, ground, and signal lines. Analog signals and DC voltages are not affected by cable length or clock speed, and should be able to transmit over several feet in this cable. The two cables are shown in Figures 30 and 31. The pinout of the 16 to 12 pin splice is detailed in Appendix B.

Figure 30. Shorter Cable Designed for Successful Programming of the MS3110 Chip.

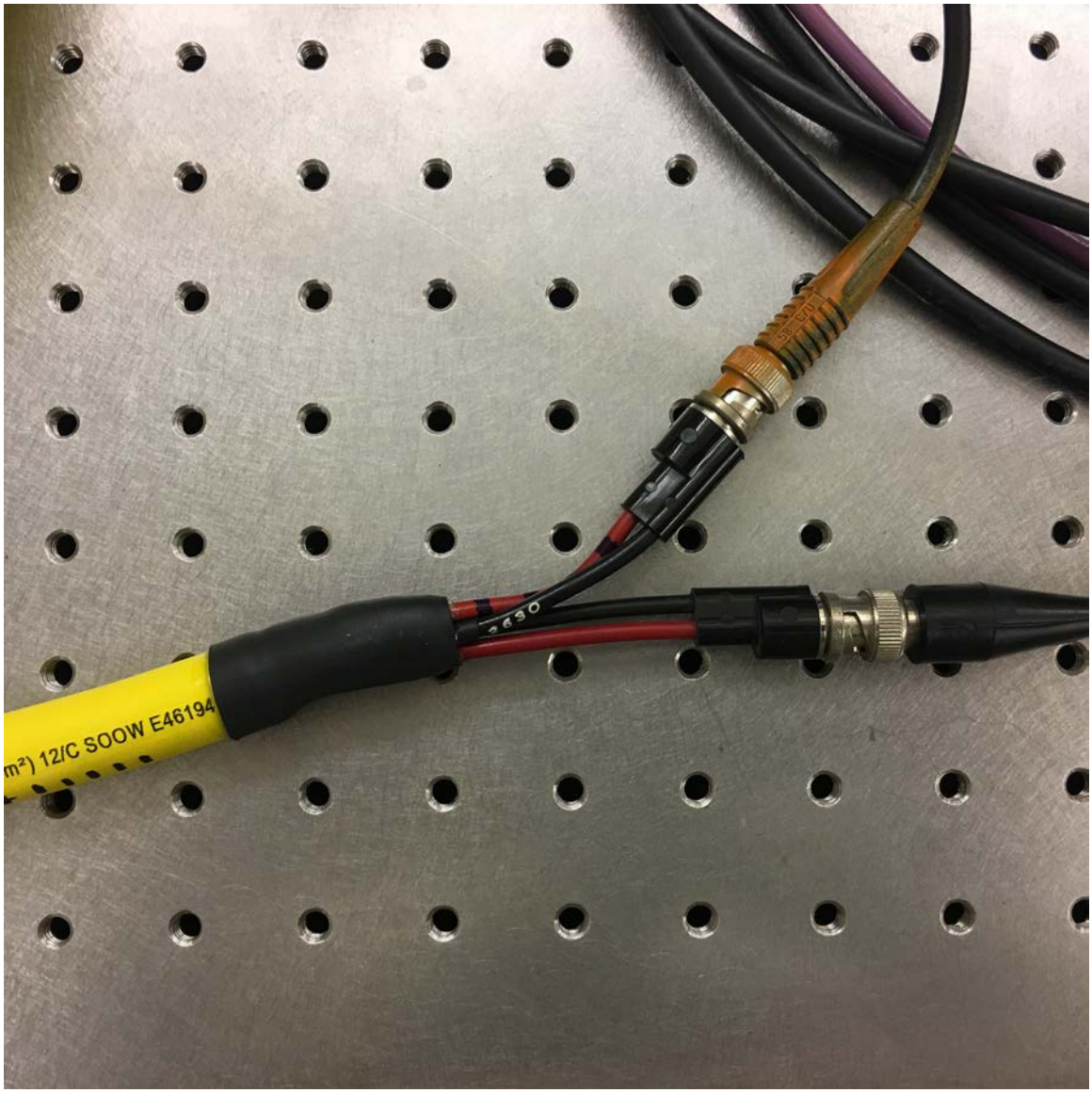

Figure 31. Longer Cable Terminates in 2 Coaxial Cables for Providing Power and Reading Sensor Output.

The chip was programmed with the new shorter programming cable. The sensor was balanced after the addition of a 10 pF capacitor across the reference leads of the MS3110 chip. This was necessary to boost the total reference capacitance feeding in to the differential capacitance measurement in order to adjust the final output to the center of the band, allowing for maximum sensitivity of the new sensor design. The MS3110 measures the difference between the wing capacitance and the fixed reference capacitor, and it outputs a corresponding voltage from 0–5V. It is desirable to tune the chip to

output 2.5 V with no sound stimulus in order to take advantage of the full range of the sensor, and also to adjust the gain so that a sound of a reasonable volume based on the expected test environment will not saturate the output. Due to the difference in total wing capacitance between the air design and the water design wings, the differential capacitance measurement made by the MS3110 chip needs to be zeroed at a higher baseline. The final settings programmed into the chip are listed in Appendix C.

B. CHARACTERIZATION OF THE NEW SENSOR IN AIR

Once the chip programming was complete, frequency response testing of the sensor in air was performed with and without the urethane cover installed. Simulations have shown that the sensor should respond to sound waves in air at a bending mode resonance around 900 Hz. The measured frequency response at normal incidence over a range of 500–1500 Hz is shown in Figure 32. The resonant frequency is found to be around 860 Hz based on that data. The slight difference between the measured and simulated responses could be due to differences in the parameters used in the simulation from the actual values after fabrication.

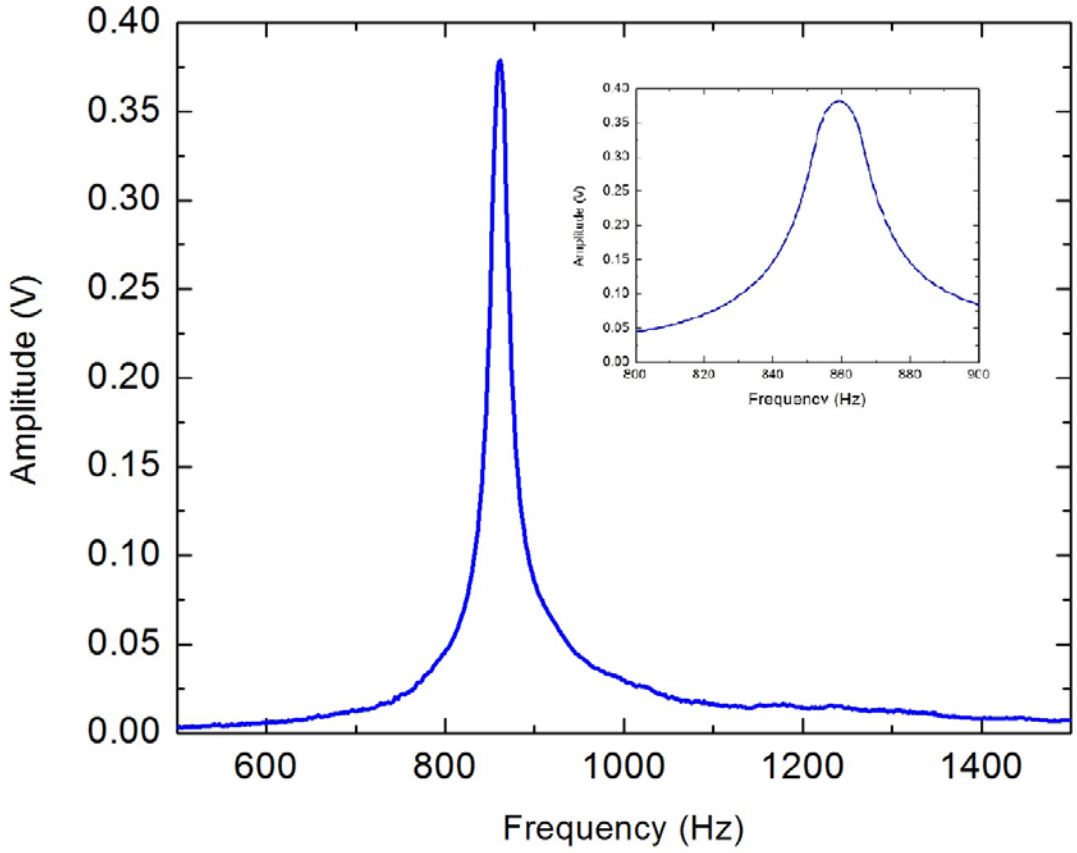

The main graph shows the frequency sweep performed from 500–1500 Hz in air at normal incidence. The inset indicates that the resonant peak of the sensor is 859 Hz.

Figure 32. Underwater Sensor Characterization in Air: 500–1500 Hz Frequency Sweep at Normal Incidence, Sound Pressure 114.6 mPa at Sensor.

Measurement of the directional response of the sensor was performed at 859 Hz, with results shown in Figure 33. The sensor shows cosine response to direction that we would expect from an open back test at the bending resonance frequency.

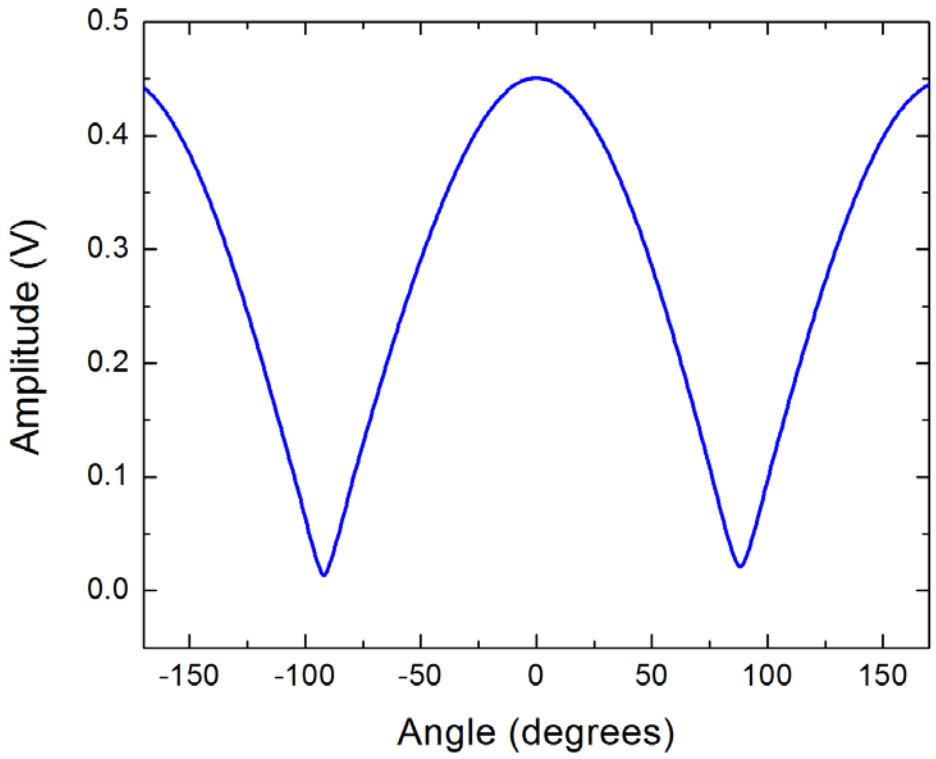

Figure 33. Underwater Sensor Characterization in Air: Rotation at 859 Hz, Sound Pressure of 114.6 mPa.

Next, the rotation test was performed with the urethane cap installed. This reduced the signal amplitude by a factor of 40, but the directional response was still cosine dependent, as shown in Figure 34. The signal is much noisier with the cap installed, likely due to a weaker sound field inside. However, increasing the time constant on the lock-in amplifier smoothed the noise sufficiently to make a direct comparison to the uncapped performance. Equipment settings for the capped and uncapped underwater sensor testing in the anechoic room are given in Appendix A.

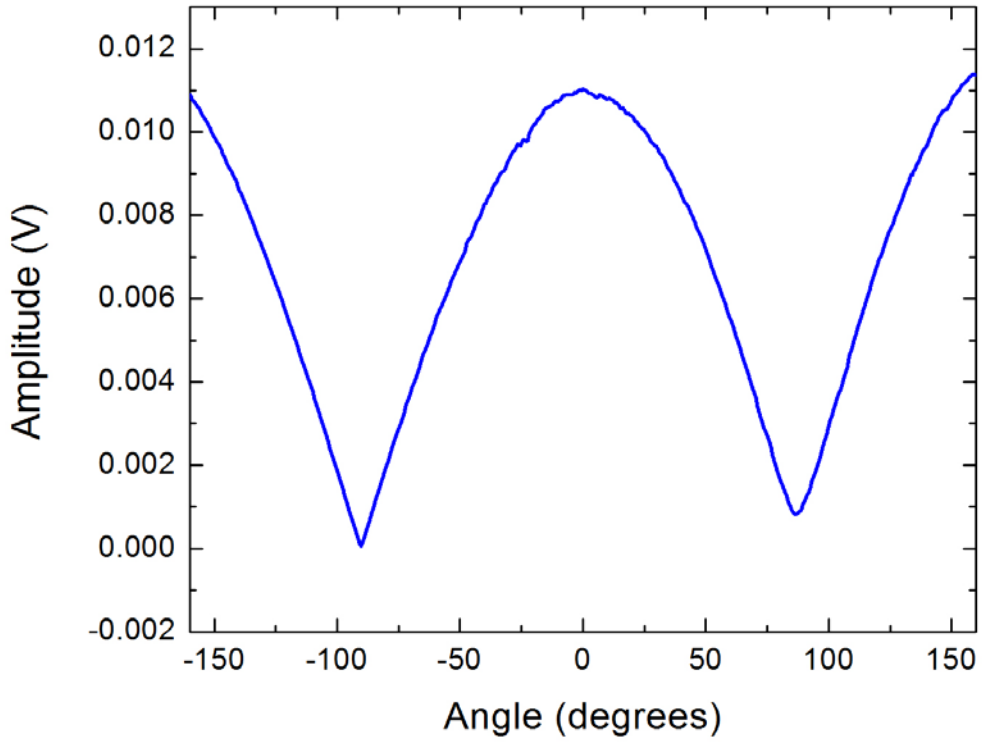

Figure 34. Underwater Sensor Characterization in Air, Cap Installed: Rotation at 859 Hz, Sound Pressure Generated is 114.6 mPa Outside Cap.

Finally, the sensitivity of the sensor at the resonant frequency with and without the urethane cap installed was measured. The same speaker voltages and reference microphone readings were used as in Chapter 2, with results shown in Table 2.

Table 2. Sensitivity of the Underwater MEMS Sensor in Air, Uncapped

Speaker output (V_{rms})	Ref Mic (mV)	Sound Pressure at sensor (mPa)	Underwater MEMS sensor in air, uncovered (mV)	UW MEMS sensitivity in air (V/Pa)
2	13.5	13.5	41	3.04
4	25.4	25.4	86	3.39
10	59.7	59.7	231	3.86
20	114.6	114.6	446	3.89

Assuming the sensor's sensitivity does not change as a result of installing the urethane cap, the measured sensor response to the same sound when the sensor is capped should give an idea of the sound transmission through the urethane in air. Table 3 shows the results of the sensitivity test for the underwater sensor with the Flexane cap installed.

Table 3. Sensitivity of the Underwater MEMS Sensor in Air, Cap Installed

Sound Pressure at sensor (mPa)	UW MEMS sensor in air, covered (mV)	Sound pressure inside cap (mPa)	Percent of sound pressure through cap
13.5	1.2	0.395	2.9%
25.4	2.3	0.678	2.7%
59.7	5.6	1.451	2.4%
114.6	10.7	2.751	2.4%

The previously calculated transmission coefficient of the urethane cap in air at 860 Hz of T = 3.4 x 10–^{3} equates to a transmission power loss of T_Π = -24.7 dB. For comparison with measurements, a calculation was carried out using the 10 V speaker output setting and corresponding sound pressure of 59.7 mPa. Often in acoustics, it is convenient to use dB scales due to the several order of magnitude variations of certain quantities within the same problem, as well as to standardize conversions between unit systems when comparing different sensor characteristics. Reference values used here are reference pressure in air, P_{ref}=20 μPa, reference voltage, V_{ref}=1 V, and reference sensitivity, M_{ref}=1 V/Pa. From [7], the Sound Pressure Level, SPL, corresponding to this pressure is

$$SPL = 20 \times \log(\frac{P_{sound}}{P_{ref}}) = 20 \times \log(\frac{59.7mPa}{20\mu Pa}) = 69.5dB, re20\mu Pa .$$

The uncapped sensor response output voltage from Table 2 yields a voltage level, VL, of

$$VL = 20 \times \log(\frac{V}{V_{ref}}) = 20 \times \log(\frac{231mV}{1V}) = -12.7dB, re1V .$$

The sensitivity level, ML, of the sensor can be obtained from

$$ML = VL - SPL + 20 \times \log(\frac{V_{ref}}{M_{ref} \cdot P_{ref}}) = -12.7 - 69.5 + 94.0 = 11.8dB, re1V / Pa .$$

Keeping ML constant for the sensor, we can subtract the calculated transmission power loss from the SPL, and then recalculate the new VL for the capped sensor.

$$VL = SPL + ML - 20 \times \log(\frac{V_{ref}}{P_{ref} \cdot M_{ref}}) - T_{\Pi} = 69.5 + 11.8 - 94 - 24.7 = -37.4 dB, re 1V .$$

This VL corresponds to a measured output voltage of V = 13.5 mV, or a difference in VL of about 6 dB, re 1V from the measured quantity. The transmission power loss could also be estimated based on the change in voltage between the capped and uncapped sensor response,

$$\Delta V = 20 \times \log(\frac{V_{capped}}{V_{uncapped}}) = 20 \times \log(\frac{5.6mV}{231mV}) = -32.3 dB ,$$

which is 7.6 dB different from the previously calculated transmission power loss, and consistent with the calculation of expected VL given above.

Based on the uncertainty in the measured sound speed of the Flexane sample as well as possible complications to the acoustic environment that the sensor sees due to reflections inside the cap, this calculation is in reasonable agreement, within one order of magnitude, with the measured result.

C. UNDERWATER PERFORMANCE

With the new MEMS underwater sensor design characterized in air and performing in good agreement with simulations, we prepared the sensor for underwater testing by filling the urethane cap with the silicon oil, placing the sensor in the oil, and bolting the backing ring to the mount. The sensor housing was mounted on the lab bench to connect to the programming board in order to check for proper communication with the circuitry and also to verify the MS3110 balance and gain settings.

The MS3110 properly communicated with the programming board via the short spliced cable and the trim capacitors were adjusted. The new settings were written into the onboard EEPROM. Final settings sent to the chip are shown in Appendix C.

The UW30 underwater speaker [15] was suspended in the NPS underwater test tank, driven by an Agilent 33220A function generator connected through a HP 467A power amplifier. Similarly, the underwater MEMS sensor was suspended in the tank 2

meters away from the UW30 speaker. The sensor power was connected to a HP E3615A DC power supply providing 5 V, and the sensor output to a Tektronix TDS 3034B Oscilloscope. With this arrangement, it was possible to manually adjust the speaker output frequency around the expected resonant point until the sensor output was visible on the oscilloscope. Figure 35 shows sensor output on the oscilloscope screen with the function generator set to 135 Hz at 1 V pk-pk, with 2X gain from the power amplifier.

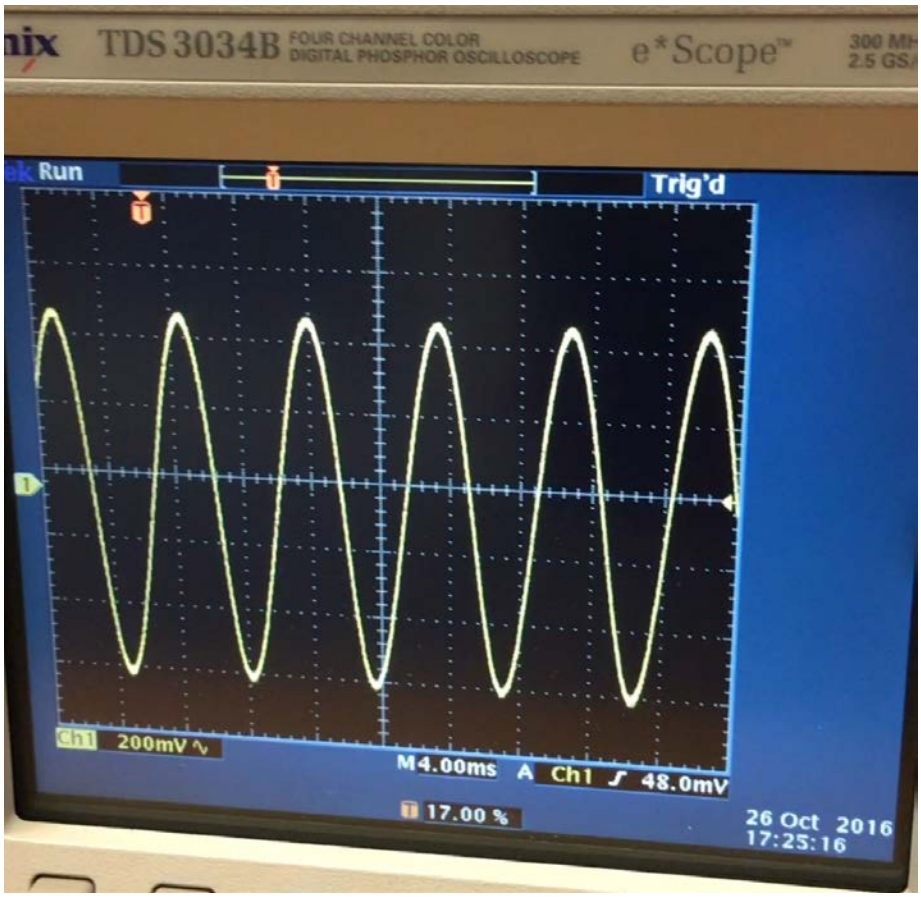

This is the Underwater MEMS sensor response to the UW30 speaker set to 135 Hz, 2V peak to peak at a distance of 2 meters.

Figure 35. Oscilloscope Screenshot from Underwater MEMS Sensor Initial Testing

Once it was verified that the sensor was providing a reasonable output to the oscilloscope, the output was connected to the SR865 Lock-In amplifier. The UW30 was driven with the sinusoidal output of the SR865 instead of the Agilent function generator.

The frequency response measurement was performed over the range 50–550 Hz and the results are shown in Figure 36. The test was repeated with a frequency range of 50–200 Hz, as shown in Figure 37, to zoom in on the resonant peaks.

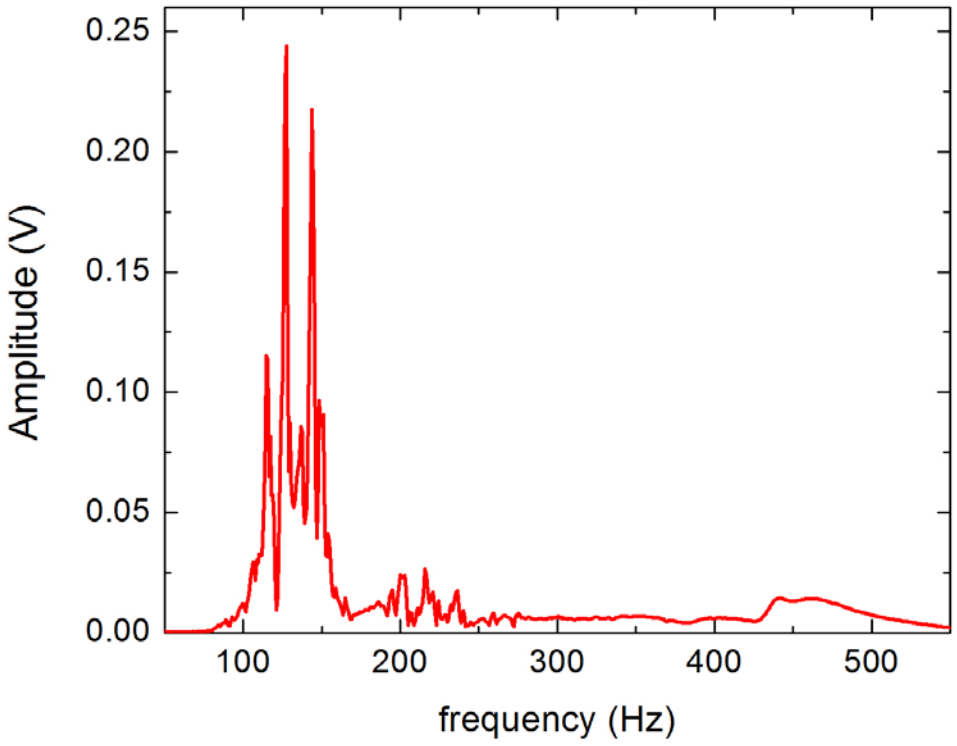

Figure 36. Underwater MEMS Sensor Test in Water, Frequency Sweep 50–550 Hz.

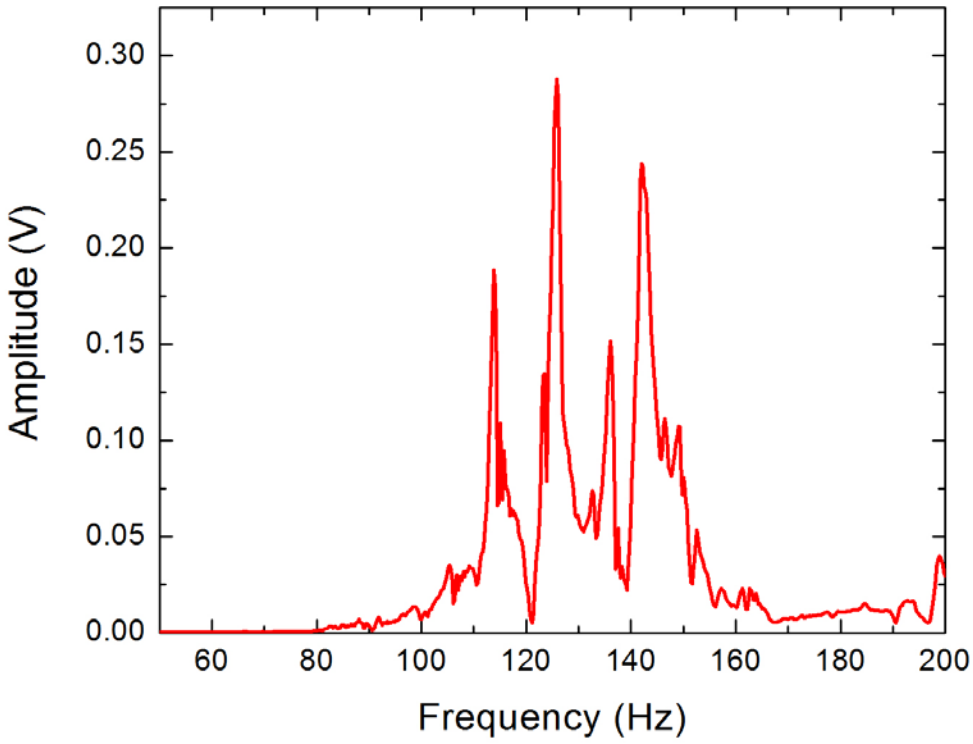

Figure 37. Underwater MEMS Sensor Test in Water, Frequency Sweep 50–200 Hz

The notable differences between the simulation and the actual measured sensor response are the appearance of multiple resonant peaks and that the resonant frequency is higher in the simulation that in the measured response. At the response frequency range 120–150 Hz, this corresponds to a wavelength around 10 meters. The speaker and the sensor are only 2 meters apart. This could lead to near-field interference patterns adding some structure to the response. Additionally, the NPS underwater tank facility is nominally only anechoic above 10 kHz, which means that any long wavelength acoustic field is going to generate significant reflections off of the bottom, sides, and surface in the tank. The UW30 speaker was generating a continuous tone, which guarantees that the acoustic field at any point in the tank is going to experience some reflections, leading to an interference pattern in the sensor response. Future testing could use short broadband chirps and a digital signal analyzer to eliminate the reflections from the response signal. A larger tank would be necessary to move the sensor into the far field to verify whether or not the shape of the measured resonant peak is fundamentally similar to the simulated

response peak. Additionally, directional response of the sensor cannot be measured in this tank until we can eliminate reflections and near-field interference as possible complications.

A MEMS acoustic DF sensor for underwater applications has been characterized in air. The acoustic properties of the newly designed housing have been verified experimentally in air. The new sensor and its underwater housing were successfully assembled, communications with the controlling electronics were verified with the sensor in the silicon oil used as fill fluid, and the sensor has been shown to respond to acoustic stimulus in water. At a sensor length scale of 10 mm, the sensor was able to detect an acoustic wave with wavelength on the order of 10 m, a factor of 1000 difference between the length scales of the sensor and the sound wave.

THIS PAGE INTENTIONALLY LEFT BLANK

V. CONCLUSIONS

A. SUMMARY OF RESULTS

Two important advancements in MEMS DF sensor technology have been demonstrated. The *Ormia ochracea* fly uses coupling between bending and rocking resonance modes of its coupled eardrums to DF a cricket. Previous MEMS sensors based on this fly have only exploited the bending mode, requiring a two sensor arrangement to compensate for utilizing only a single resonant mode. Incorporating an enclosure behind the sensor to more closely reproduce the fly's hearing system has allowed our sensors, for the first time, to identify the rocking resonant mode and use it for acoustic DF sensing. Changing the readout configuration should allow single sensor DF with a high accuracy in a smaller package.

Additionally, an underwater version of the MEMS DF acoustic sensor based on the *Ormia* hearing system has been designed and fabricated, along with an appropriate underwater housing. Successful testing of this sensor's response to acoustic stimulus underwater demonstrates that MEMS acoustic sensors represent a practical approach to small form factor directional acoustic sensing, even accounting for the significantly longer wavelengths of sound in the water.

This will lead to the ability to create small, low power, accurate underwater acoustic DF sensors that can be designed to be sensitive to specific frequencies based on application. This will be an improvement over existing underwater directional sensors because of its small size and narrow band resonant response.

The benefits to the Navy of these new sensor designs includes the creation of an air sensor that is in a smaller form-factor package, that is functional for DF over a wider angle, and that includes fewer electronics. The benefits of creating a water-based sensor include the ability to install a low-cost, low-power, narrow-band directional sensor across a variety of platforms, and that, at the time of manufacture, can be tuned to a desired frequency.

B. RECOMMENDATIONS FOR FUTURE WORK

The improvements to the air based sensor demonstrated here represent a critical step in understanding the rocking resonant mode. Theoretical as well as modeling and simulation work will be necessary to understand why opening the back of the sensor to the air causes the rocking mode to be suppressed.

The parallel two sensor configuration tested in this thesis satisfactorily demonstrated that the rocking mode is measureable and useful, but still required two sensors. Fabricating a sensor that is wired to present the difference capacitance between the wings as the input to the MS3110 chip, rather than the difference between the wing and the fixed reference capacitor, is a necessary next step to demonstrating true single sensor DF capability.

Additional testing of the underwater sensor will require new equipment and a larger test facility. At the resonant frequency of this design, greater separation between the speaker and sensor are required to ensure the sensor is in the far field of an omnidirectional driver like the UW30. Also, sensitivity measurements by the standard reciprocity calibration method [7] would require low frequency equipment that NPS does not currently have possess. The Type F33 transducer, for instance, that NPS uses for reciprocity calibrations is not useful below 1 kHz [16]. Another solution to this issue would be to design an underwater sensor that resonates on the order of 10^5 Hz in water. Then the existing equipment at NPS could be used to fully characterize these new sensors, including sensitivity and directionality.

It is evident upon visual inspection of the underwater sensors under microscope that the wing is bent up away from the substrate at rest, due to residual stress remaining after the substrate was trenched away from the back side of the sensor. This is not entirely unexpected, given the size and thickness of the device. SEM imaging will be necessary to evaluate the magnitude of the deflection due to the residual stress, as well as whether it is a consistent amount of stress across all of the sensors created on the wafer. Options for future design include deposition of a stress compensation layer on the sensor that would be designed to apply stress in the opposite direction and leave the sensor in the

plane of the substrate at rest [17]. This is an extra step that could be added in conjunction with assumption of fabrication of this sensor in the NPS clean room facility, but is not available within the SOIMUMPS production steps [6].

Finally, after either the sensors are redesigned for a higher resonant frequency or the facilities are altered to allow testing of low frequency equipment at NPS, and the sensors can be fully characterized, then directionality can be demonstrated in accordance with simulations.

THIS PAGE LEFT INTENTIONALLY BLANK

APPENDIX A. LOCK-IN AND PREAMP SETTINGS

A. OPEN BACK DUAL PARALLEL SENSOR SETUP

1. SR865 Lock-in Amplifier Settings

Sensitivity: 100 mV

Time Constant: 10 msec

Range: 100mV

Filter: 6dB slope

Sweep time: 100 sec

2. HP467A Power Amplifier Output to Speaker

Lock-in output set to 1 V pk-pk with 5X gain from amplifier

B. CLOSED BACK DUAL PARALLEL SENSOR SETUP

1. SR865 Lock-in Amplifier Settings

Sensitivity: 100 mV

Time Constant: 30 msec

Range: 300mV

Filter: 6dB slope

Sweep time: 100 sec

2. HP467A Power Amplifier Output to Speaker

Lock-in output set to 1 V pk-pk with 10X gain from amplifier

3. SR560 Low-Noise Pre-Amp Settings

Filter: 6dB slope

High pass: 300 Hz

Low pass: 3KHz

Gain: 10X

Low noise

C. UNDERWATER SENSOR – AIR TEST WITHOUT CAP

1. SR865 Lock-in Amplifier Settings

Sensitivity: 100 mV

Time Constant: 30 msec

Range: 300mV

Filter: 6dB slope

Sweep time: 100 sec

2. HP467A Power Amplifier Output to Speaker

Lock-in output set to 2 V pk-pk with 10X gain from amplifier

D. UNDERWATER SENSOR – AIR TEST WITH CAP

1. SR865 Lock-in Amplifier Settings

Sensitivity: 10 mV

Time Constant: 300 msec

Range: 100mV

Filter: 6dB slope

Sweep time: 100 sec

2. HP467A Power Amplifier Output to Speaker

Lock-in output set to 2 V pk-pk with 10X gain from amplifier

E. UNDERWATER SENSOR – WATER SETUP

1. SR865 Lock-in Amplifier Settings

Sensitivity: 500 mV

Time Constant: 100 msec

Range: 1 V

Filter: 6dB slope

Sweep time: 100 sec

2. HP467A Power Amplifier Output to Speaker

Lock-in output set to 1 V pk-pk with 1X gain from amplifier

THIS PAGE INTENTIONALLY LEFT BLANK

APPENDIX B. UNDERWATER SIGNAL CABLE TO RIBBON CABLE SPLICE WIRING CHART

A. RIBBON CABLE

Pin #	Pin	Pin	Pin#
1 (red)	HV16	--	2
3	--	V2P25	4
5	+V	--	6
7	TESTSEL	--	8
9	V OUT	--	10
11	-V GND	CHPRST	12
13	--	SCLK	14
15	WBT	SDATA	16

B. UW CABLE

1	RED/BLACK
4	WHITE/BLACK
5	BLUE
7	ORANGE
9	RED
11	GREEN
12	GREEN/BLACK
14	BLACK/WHITE
15	ORANGE/BLACK
16	BLUE/BLACK

THIS PAGE INTENTIONALLY LEFT BLANK

APPENDIX C. MS3110 SETTINGS

A. AIR SENSOR, DUAL PARALLEL ARRAY, BACK CLOSED

Current Reference Trim	Nominal
Voltage Reference Trim	Nominal
Oscillator Trim	Nominal
Output Buffer Gain Trim	Nominal
Output Buffer Offset Trim	Nominal
Output Buffer Output Offset Level Control	2.25V
Continuous-Time LPF Bandwidth Trim	3.0 KHz
Output Buffer Gain Select	4
IAMP Feedback Capacitor Selection	3.268 pF
IAMP Balance Capacitor Trim	1.235 pF
IAMP Balance Trim Capacitor Selection	0.095 pF

B. UNDERWATER SENSOR

Current Reference Trim	Nominal
Voltage Reference Trim	Nominal
Oscillator Trim	Nominal
Output Buffer Gain Trim	Nominal
Output Buffer Offset Trim	Nominal
Output Buffer Output Offset Level Control	2.25V
Continuous-Time LPF Bandwidth Trim	3.0 KHz
Output Buffer Gain Select	4

IAMP Feedback Capacitor Selection	2.014 pF
IAMP Balance Capacitor Trim	8.151 pF
IAMP Balance Trim Capacitor Selection	0.171 pF

LIST OF REFERENCES

[1] J. Blauert, *Spatial Hearing: The Psychophysics of Human Sound Localization*, 2nd ed. Cambridge, MA: MIT Press, 1996.

[2] R. Miles, D. Robert, and R. Hoy, "Mechanically coupled ears for directional hearing in the parasitoid fly *Ormia ochracea*," *J. Acoust. Soc. Am.*, vol. 98, no. 6, pp. 3059–3070, Dec. 1995.

[3] M. Touse, J. Sinibaldi, K. Simsek, J. Catterlin, S. Harrison, and G. Karunasiri, "Fabrication of a microelectromechanical directional sound sensor with electronic readout using comb fingers," *Appl. Physics Lett.*, vol. 96, no. 17, 2010.

[4] D. Wilmott, "Direction Finding Using Multiple MEMS Acoustic Sensors," M.S. thesis, Dept. of Physics, Naval Postgraduate School, Monterey, CA, 2015.

[5] J. Roth, "Integration of a high sensitivity MEMS directional sound sensor with readout electronics," M.S. thesis, Dept of Physics, Naval Postgraduate School, Monterey, CA, 2009.

[6] MEMSCAP: SOIMUMPs and MEMS Multi Project Wafer Service. (n.d.). MEMSCAP. [Online]. Available: http://www.memscap.com/products/mumps/soimumps/. Accessed October 30, 2016.

[7] L. Kinsler, A. Frey, A. Coppens, and J. Sanders, *Fundamentals of Acoustics*, 4th ed., Hoboken, NJ: John Wiley & Sons, 2012.

[8] SR865 2MHz DSP Lock-in Amplifier Operation Manual, Rev 1.29, Stanford Research Systems, Sunnyvale, CA, 2015.

[9] G. Jebsen, "Acoustic Diffraction by a Finite Barrier: Theories and Experiment," M.S. thesis, Dept of Physics, Naval Postgraduate School, Monterey, CA, 1981.

[10] Product Data – 1/8" Pressure-Field Microphone – Type 4138. (2008, Sept.). Brüel & Kjær. [Online]. Available: https://www.bksv.com/~/media/literature/Product%20Data/bp2030.ashx

[11] Flexane 80 Liquid Technical Data Sheet. (2012, Apr. 17). Devcon. [Online]. Available: http://www.devcon.com/prodfiles/pdfs/fam_tds_151.pdf

[12] O. Wilson, *Introduction to Theory and Design of Sonar Transducers*, 2nd ed. Los Altos, CA: Peninsula Publishing, 1988.

[13] Delrin Data Sheet. (2003, Mar.). Ensinger-Hyde. [Online]. Available: http://www.sdplastics.com/delrin/delrin[1].pdf

[14] *COMSOL Multiphysics*, version 5.2, COMSOL, Burlington, MA, 2016.

[15] UW30 Engineering Data Sheet (2010, Feb.). Electro-Voice. [Online]. Available: http://www.electrovoice.com/downloadfile.php?i=1526

[16] Type F33 Transducer Data Sheet (1994, Aug.) Naval Sea Systems Command. [Online]. Available: http://www.navsea.navy.mil/Portals/103/Documents/NUWC_Newport/USRD/F33.pdf

[17] C. Liu, *Foundations of MEMS*, 2nd ed. Upper Saddle River, NJ: Pearson Education, 2011.

INITIAL DISTRIBUTION LIST

1. Defense Technical Information Center
   Ft. Belvoir, Virginia

2. Dudley Knox Library
   Naval Postgraduate School
   Monterey, California